INSTITUTE OF PHYSICS PUBLISHING INVERSE PROBLEMS

Inverse Problems **18** (2002) R99–R136 PII: S0266-5611(02)95228-7

TOPICAL REVIEW

Electrical impedance tomography

Liliana Borcea

Computational and Applied Mathematics, MS 134, Rice University, 6100 Main Street, Houston, TX 77005-1892, USA

E-mail: borcea@caam.rice.edu

Received 16 May 2002, in final form 4 September 2002
Published 25 October 2002
Online at stacks.iop.org/IP/18/R99

Abstract

We review theoretical and numerical studies of the inverse problem of electrical impedance tomography which seeks the electrical conductivity and permittivity inside a body, given simultaneous measurements of electrical currents and potentials at the boundary.

(Some figures in this article are in colour only in the electronic version)

1. Introduction

Electrical properties such as the electrical conductivity σ and the electric permittivity ϵ, determine the behaviour of materials under the influence of external electric fields. For example, conductive materials have a high electrical conductivity and both direct and alternating currents flow easily through them. Dielectric materials have a large electric permittivity and they allow passage of only alternating electric currents.

Let us consider a bounded, simply connected set $\Omega \subset \mathbb{R}^d$, for $d \geqslant 2$ and, at frequency ω, let γ be the complex admittivity function

$$\gamma(\boldsymbol{x}, \omega) = \sigma(\boldsymbol{x}) + \mathrm{i}\omega\epsilon(\boldsymbol{x}), \qquad \text{where } \mathrm{i} = \sqrt{-1}. \tag{1.1}$$

The electrical impedance is the inverse of $\gamma(\boldsymbol{x})$ and it measures the ratio between the electric field and the electric current at location $\boldsymbol{x} \in \Omega$. Electrical impedance tomography (EIT) is the inverse problem of determining the impedance in the interior of Ω, given simultaneous measurements of direct or alternating electric currents and voltages at the boundary $\partial\Omega$.

Different materials display different electrical properties, as shown in tables 1 and 2, so a map of $\sigma(\boldsymbol{x})$ and $\epsilon(\boldsymbol{x})$, for $\boldsymbol{x} \in \Omega$, can be used to infer the internal structure in Ω. Due to this fact, EIT is an imaging tool with important applications in fields such as medicine, geophysics, environmental sciences and nondestructive testing of materials. Examples of medical applications of EIT are the detection of pulmonary emboli [39, 83, 84], monitoring of apnoea [1], monitoring of heart functionand bloodflow [70, 89] andbreast cancer detection[39]. In geophysics and environmental sciences, EIT can be useful for locating underground mineral deposits [123], detection of leaks in underground storage tanks [124] and for monitoring flows

Table 1. Electrical properties of biological tissue measured at frequency 10 kHz [10, 131].

Tissue	$1/\sigma$ (Ω cm)	ϵ (μF m^{-1})
Lung	950	0.22
Muscle	760	0.49
Liver	685	0.49
Heart	600	0.88
Fat	>1000	0.18

Table 2. Resistivity of rocks and fluids [99].

Rock or fluid	$1/\sigma$ (Ω cm)
Marine sand, shale	1–10
Terrestrial sands, claystone	15–50
Volcanic rocks, basalt	10–200
Granite	500–2000
Limestone dolomite, anhydrite	50–5000
Chloride water from oil fields	0.16
Sulfate water from oil fields	1.2

of injected fluids into the earth, for the purpose of oil extraction or environmental cleaning [125]. Finally, in nondestructive testing, EIT can be used for the detection of corrosion [127] and of small defects, such as cracks or voids, in metals [5, 6, 34, 63, 71, 129].

EIT has been studied extensively in the last two decades and substantial progress has been made in both the theoretical and applied aspects of the problem. At the same time, EIT remains an area of active research and it continues to pose a variety of challenging questions for theoreticians, numerical analysts and experimentalists alike. This paper is a survey of some mathematical results about the EIT problem. We review theoretical works on uniqueness of solutions, given full knowledge of the voltage to current (Dirichlet-to-Neumann) map, as well as the continuous dependence (or lack of it) of solutions, on the boundary data. A strong emphasis is put on numerical reconstructions of function γ, in the interior of Ω. For issues of experimental design, which are briefly mentioned but largely ignored in this survey, we refer the reader to works such as [39, 135] (and the references within).

The paper is organized as follows: in section 2, we describe the mathematical model for EIT. Basically, all of the surveyed results assume a simple, continuum model for the boundary excitation. However, for completeness, we give a brief description of some of the proposed electrode models, as well. In section 3, we formulate the inverse EIT problem. We define the Dirichlet-to-Neumann (DtN) and Neumann-to-Dirichlet (NtD) maps and we review some of their properties, including their variational formulations. In section 4, we review the injectivity of the forward map. High-contrast EIT is reviewed in section 5. Even though uniqueness of solutions of the inverse problem holds for a large class of admittivity functions (section 4), the inverse map is typically discontinuous and the EIT problem is ill-posed, as we discuss in section 6. Numerical reconstruction algorithms are reviewed in section 7. Some brief references to other problems related to EIT are made in section 8. Finally, in section 9, we present conclusions and a few suggestions for future work.

2. The mathematical model

Time-harmonic electric and magnetic fields

$$\mathcal{E}(x,t) = \mathrm{Re}\{E(x,\omega)\mathrm{e}^{\mathrm{i}\omega t}\}, \qquad \mathcal{H}(x,t) = \mathrm{Re}\{H(x,\omega)\mathrm{e}^{\mathrm{i}\omega t}\},$$

satisfy Maxwell's equations

$$\begin{aligned} \nabla \times H(x,\omega) &= \gamma(x,\omega)E(x,\omega), \\ \nabla \times E(x,\omega) &= -\mathrm{i}\omega\mu(x)H(x,\omega), \end{aligned} \tag{2.1}$$

where $\mu(x)$ is the magnetic permeability and $\mathrm{Re}\{f\}$ denotes the real part of a complex function f. EIT operates at low frequencies ω, in a regime with admittivities γ and length scales L satisfying $\omega\mu|\gamma|L^2 \ll 1$, such that, after a simple scaling analysis [39], equations (2.1) are approximated by

$$\begin{aligned} \nabla \times H(x,\omega) &= \gamma(x,\omega)E(x,\omega), \\ \nabla \times E(x,\omega) &= 0. \end{aligned} \tag{2.2}$$

We define the scalar electric potential ϕ and the vector-valued, time-harmonic electric current density $\mathcal{I}(x,t) = \mathrm{Re}\{j(x,\omega)\mathrm{e}^{\mathrm{i}\omega t}\}$, as

$$E(x,\omega) = -\nabla\phi(x,\omega), \qquad \nabla \times H(x,\omega) = j(x,\omega), \tag{2.3}$$

such that the first equation in (2.2) becomes Ohm's law

$$j(x) = -\gamma(x,\omega)\nabla\phi(x,\omega). \tag{2.4}$$

Note that the density of dissipated energy, averaged over a period of oscillations,

$$\begin{aligned} \frac{\omega}{2\pi}\int_t^{t+\frac{2\pi}{\omega}} \mathcal{I}(x,\tau)\cdot\mathcal{E}(x,\tau)\,\mathrm{d}\tau &= \frac{1}{2}[\mathrm{Re}\{j(x,\omega)\}\cdot\mathrm{Re}\{E(x,\omega)\} \\ &\quad + \mathrm{Im}\{j(x,\omega)\}\cdot\mathrm{Im}\{E(x,\omega)\}] = \tfrac{1}{2}\sigma(x)|\nabla\phi(x,\omega)|^2 \end{aligned}$$

must be strictly positive, so we require that

$$\sigma(x) = \mathrm{Re}\{\gamma(x,\omega)\} \geqslant m > 0. \tag{2.5}$$

The majority of the reviewed results assume isotropic materials with admittivity $\gamma(x,\omega)$ a scalar-valued, $L^\infty(\overline{\Omega})$ function, where $\overline{\Omega}$ is the closure of the domain. Nevertheless, some theoretical studies for anisotropic materials are mentioned as well (see section 4.4).

2.1. The continuum model

By definition, j is divergence free so Ohm's law (2.4) gives the partial differential equation

$$\nabla\cdot[\gamma(x,\omega)\nabla\phi(x,\omega)] = 0 \qquad \text{in } \Omega, \tag{2.6}$$

which we take with either Dirichlet boundary conditions

$$\phi(x,\omega) = V(x,\omega), \qquad \text{for } x \in \partial\Omega, \tag{2.7}$$

or Neumann boundary conditions

$$\begin{aligned} \gamma(x,\omega)\nabla\phi(x,\omega)\cdot n(x) \equiv \gamma(x,\omega)\frac{\partial\phi(x,\omega)}{\partial n} &= I(x,\omega) \qquad \text{at } \partial\Omega, \\ \text{such that } \int_{\partial\Omega} I(x,\omega)\,\mathrm{d}s(x) &= 0, \end{aligned} \tag{2.8}$$

where $n(x)$ is the outer normal at $x \in \partial\Omega$.

Assuming (2.5) and $\gamma(\boldsymbol{x},\omega)\in L^\infty(\overline{\Omega})$, the Dirichlet boundary value problem (2.6), (2.7), for arbitrary $V\in H^{\frac{1}{2}}(\partial\Omega)$, has a unique solution $\phi(\boldsymbol{x},\omega)\in H^1(\Omega)$, at least in the weak sense [68]. The Neumann boundary value problem (2.6), (2.8), for $I\in H^{-\frac{1}{2}}(\partial\Omega)$, has a unique solution $\phi(\boldsymbol{x},\omega)\in H^1(\Omega)$, up to an additive constant [68], which we fix by choosing the ground as

$$\int_{\partial\Omega}\phi(\boldsymbol{x},\omega)\,\mathrm{d}s(\boldsymbol{x})=\int_{\partial\Omega}V(\boldsymbol{x},\omega)\,\mathrm{d}s(\boldsymbol{x})=0. \tag{2.9}$$

The electric current density satisfies equations

$$\begin{gathered}\nabla\times\left[\frac{1}{\gamma(\boldsymbol{x},\omega)}\boldsymbol{j}(\boldsymbol{x},\omega)\right]=0\qquad\text{and}\qquad\nabla\cdot\boldsymbol{j}(\boldsymbol{x},\omega)=0\qquad\text{in }\Omega,\\ -\boldsymbol{j}(\boldsymbol{x},\omega)\cdot\boldsymbol{n}(\boldsymbol{x})=I(\boldsymbol{x},\omega),\qquad\text{for }\boldsymbol{x}\in\partial\Omega,\qquad\text{such that}\int_{\partial\Omega}I(\boldsymbol{x},\omega)\,\mathrm{d}s(\boldsymbol{x})=0,\end{gathered} \tag{2.10}$$

which, by (2.4), are equivalent to (2.6), (2.8). In particular, we have that (2.10) has a unique solution $\boldsymbol{j}(\boldsymbol{x},\omega)\in L^2(\Omega)$, which is related to electric potential $\phi(\boldsymbol{x},\omega)\in H^1(\Omega)$, a solution of (2.6), (2.8), by Ohm's law (2.4).

Boundary value problems (2.6), (2.7); (2.6), (2.8) or, equivalently, (2.10), for a known function $\gamma(\boldsymbol{x},\omega)$ in Ω and data $I(\boldsymbol{x},\omega)$ or $V(\boldsymbol{x},\omega)$, given for all $\boldsymbol{x}\in\partial\Omega$, are referred to as *continuum, forward* mathematical models for EIT.

2.2. Modelling the electrodes

In practice, we do not know boundary current $I(\boldsymbol{x},\omega)$ for all $\boldsymbol{x}\in\partial\Omega$. What we actually know are currents sent along wires which are attached to N discrete electrodes, which in turn are attached to the boundary $\partial\Omega$ [135]. Then, the question is how to model the electrodes?

The *gap model* approximates the current density by a constant at the surface of each electrode and by zero in the gaps between the electrodes. This model is appealing because of its simplicity but it is not accurate [90]. A better choice is the *complete model* proposed in [135]. Suppose that $I_l(\omega)$ is the electric current sent through the wire attached to the lth electrode. At the surface S_l of this electrode, the normal current density satisfies

$$\int_{S_l}\gamma(\boldsymbol{x},\omega)\frac{\partial\phi(\boldsymbol{x},\omega)}{\partial n}\,\mathrm{d}s(\boldsymbol{x})=I_l(\omega). \tag{2.11}$$

In the gaps between the electrodes, we have

$$\gamma(\boldsymbol{x},\omega)\frac{\partial\phi(\boldsymbol{x},\omega)}{\partial n}=0. \tag{2.12}$$

At the contact of S_l with $\partial\Omega$, there is an electro-chemical effect which gives rise to a thin, highly resistive layer. This is taken into account by the surface impedance $z_l(\omega)$ and

$$\phi(\boldsymbol{x},\omega)+z_l(\omega)\gamma(\boldsymbol{x},\omega)\frac{\partial\phi(\boldsymbol{x},\omega)}{\partial n}=V_l(\omega)\qquad\text{for }\boldsymbol{x}\in S_l,\ l=1,\dots N, \tag{2.13}$$

where $V_l(\omega)$ is the measured voltage at the lth electrode. Finally, due to conservation of charge and, by the choice of ground,

$$\sum_{l=1}^{N}I_l(\omega)=\sum_{l=1}^{N}V_l(\omega)=0. \tag{2.14}$$

It is proved in [135] that equations (2.6), (2.11)–(2.14) have a unique solution and that they predict experimental data with errors less than 1%. However, this complete model is more complicated than the continuum one and the inverse problem based on it remains essentially unstudied from the theoretical and numerical reconstructions points of view. Consequently, in the remainder of this survey, we concentrate on the continuum model.

3. Formulation of the inverse problem

In EIT, the admittivity function $\gamma(\boldsymbol{x}, \omega)$ is unknown and it is to be determined from simultaneous measurements of boundary voltages $V(\boldsymbol{x}, \omega)$ and current densities $I(\boldsymbol{x}, \omega)$, respectively. In this section, we define the DtN and NtD maps which relate $V(\boldsymbol{x}, \omega)$ to $I(\boldsymbol{x}, \omega)$. These maps depend nonlinearly on the unknown $\gamma(\boldsymbol{x}, \omega)$ and they are data in inversion. We review some properties of these maps and we formulate the inverse problem.

3.1. The Dirichlet-to-Neumann and the Neumann-to-Dirichlet maps

The DtN map $\Lambda_\gamma : H^{\frac{1}{2}}(\partial\Omega) \to H^{-\frac{1}{2}}(\partial\Omega)$ is defined as

$$\Lambda_\gamma V(\boldsymbol{x}, \omega) = \gamma(\boldsymbol{x}, \omega)\frac{\partial\phi(\boldsymbol{x}, \omega)}{\partial n} \qquad \text{for } \boldsymbol{x} \in \partial\Omega, \tag{3.1}$$

where $V(\boldsymbol{x}, \omega)$ is arbitrary in $H^{\frac{1}{2}}(\partial\Omega)$ and $\phi(\boldsymbol{x}, \omega)$ solves forward problem (2.6), (2.7).

Suppose that potentials $\phi(\boldsymbol{x}, \omega)$ and $\psi(\boldsymbol{x}, \omega)$ are solutions of boundary value problem (2.6), (2.7), for Dirichlet data $V(\boldsymbol{x}, \omega)$ and $W(\boldsymbol{x}, \omega)$ in $H^{\frac{1}{2}}(\partial\Omega)$, respectively. We define the inner product

$$\langle f, g\rangle = \int_{\partial\Omega} f^\star(\boldsymbol{x}) g(\boldsymbol{x})\, \mathrm{d}s(\boldsymbol{x}),$$

where $f^\star(\boldsymbol{x})$ is the complex conjugate of $f(\boldsymbol{x})$, and we have

$$\begin{aligned}
\langle W, \Lambda_\gamma V\rangle &= \int_{\partial\Omega} W^\star(\boldsymbol{x}, \omega)\gamma(\boldsymbol{x}, \omega)\frac{\partial\phi(\boldsymbol{x}, \omega)}{\partial n}\, \mathrm{d}s(\boldsymbol{x}) \\
&= \int_\Omega \gamma(\boldsymbol{x}, \omega)\nabla\phi(\boldsymbol{x}, \omega)\cdot\nabla\psi^\star(\boldsymbol{x}, \omega)\, \mathrm{d}\boldsymbol{x}, \\
\langle \Lambda_\gamma W, V\rangle &= \int_{\partial\Omega} V(\boldsymbol{x}, \omega)\gamma^\star(\boldsymbol{x}, \omega)\frac{\partial\psi^\star(\boldsymbol{x}, \omega)}{\partial n}\, \mathrm{d}s(\boldsymbol{x}) \\
&= \int_\Omega \gamma^\star(\boldsymbol{x}, \omega)\nabla\phi(\boldsymbol{x}, \omega)\cdot\nabla\psi^\star(\boldsymbol{x}, \omega)\, \mathrm{d}\boldsymbol{x}.
\end{aligned} \tag{3.2}$$

In particular, if we let $V(\boldsymbol{x}, \omega) = W(\boldsymbol{x}, \omega)$ in (3.2), we observe that $\langle V, \Lambda_\gamma V\rangle = 0$ if and only if $\nabla\phi(\boldsymbol{x}, \omega) = 0$ almost everywhere in Ω (recall assumption (2.5)). Hence, the DtN map has a nontrivial null space: $\mathrm{null}\{\Lambda_\gamma\} = \{V(\boldsymbol{x}, \omega) = \text{constant}\}$.

In the static case $\omega = 0$, we have $\gamma(\boldsymbol{x}, 0) = \sigma(\boldsymbol{x})$ and $\Lambda_\gamma \equiv \Lambda_\sigma$ satisfies the following lemma.

Lemma 1. *Λ_σ is a self-adjoint, positive semidefinite map with variational formulation*

$$\langle V, \Lambda_\sigma V\rangle = \min_{u|_{\partial\Omega}=V} \int_\Omega \sigma(\boldsymbol{x})|\nabla u(\boldsymbol{x})|^2\, \mathrm{d}\boldsymbol{x}, \qquad \textit{for arbitrary } V(\boldsymbol{x}) \in H^{\frac{1}{2}}(\partial\Omega). \tag{3.3}$$

The self-adjointness of Λ_σ follows immediately from (3.2) and the Dirichlet variational principle (3.3) can be found, for example, in [44].

When $\omega \neq 0$, Λ_γ is complex-symmetric but not self-adjoint, and it has the following variational formulation.

Lemma 2. *Let the boundary potential be $V(\boldsymbol{x}, \omega) = V_{\mathrm{R}}(\boldsymbol{x}, \omega) + \mathrm{i}V_{\mathrm{I}}(\boldsymbol{x}, \omega)$, where V_{R} and V_{I} are real-valued functions in $H^{\frac{1}{2}}(\partial\Omega)$. Then,*

$$\begin{aligned}
\mathrm{Re}\langle V^\star, \Lambda_\gamma V\rangle &= \min_{u_{\mathrm{R}}|_{\partial\Omega}=V_{\mathrm{R}}} \max_{u_{\mathrm{I}}|_{\partial\Omega}=V_{\mathrm{I}}} \int_\Omega \mathrm{Re}\{\gamma\nabla(u_{\mathrm{R}} + \mathrm{i}u_{\mathrm{I}})\cdot\nabla(u_{\mathrm{R}} + \mathrm{i}u_{\mathrm{I}})\}\, \mathrm{d}\boldsymbol{x} \\
&= \min_{u_{\mathrm{R}}|_{\partial\Omega}=V_{\mathrm{R}}} \max_{u_{\mathrm{I}}|_{\partial\Omega}=V_{\mathrm{I}}} \int_\Omega (\nabla u_{\mathrm{R}}, \nabla u_{\mathrm{I}}) \begin{pmatrix} \sigma & -\omega\epsilon \\ -\omega\epsilon & -\sigma \end{pmatrix} \begin{pmatrix} \nabla u_{\mathrm{R}} \\ \nabla u_{\mathrm{I}} \end{pmatrix} \mathrm{d}\boldsymbol{x},
\end{aligned} \tag{3.4}$$

and

$$\operatorname{Im}\langle V^\star, \Lambda_\gamma V\rangle = \min_{u_{\mathrm{R}}|_{\partial\Omega}=V_{\mathrm{R}}} \max_{u_{\mathrm{I}}|_{\partial\Omega}=V_{\mathrm{I}}} \int_\Omega \operatorname{Im}\{\gamma\nabla(u_{\mathrm{R}}+\mathrm{i}u_{\mathrm{I}})\cdot\nabla(u_{\mathrm{R}}+\mathrm{i}u_{\mathrm{I}})\}\,\mathrm{d}\boldsymbol{x}$$

$$= \min_{u_{\mathrm{R}}|_{\partial\Omega}=V_{\mathrm{R}}} \max_{u_{\mathrm{I}}|_{\partial\Omega}=V_{\mathrm{I}}} \int_\Omega (\nabla u_{\mathrm{R}}, \nabla u_{\mathrm{I}}) \begin{pmatrix} \omega\epsilon & \sigma \\ \sigma & -\omega\epsilon \end{pmatrix} \begin{pmatrix} \nabla u_{\mathrm{R}} \\ \nabla u_{\mathrm{I}} \end{pmatrix} \mathrm{d}\boldsymbol{x}. \tag{3.5}$$

Variational principles (3.4) and (3.5) are derived and analysed in [40, 67]. Note that, at the saddle point, functions $u_{\mathrm{R}}(\boldsymbol{x},\omega)$ and $u_{\mathrm{I}}(\boldsymbol{x},\omega)$ in (3.4) and (3.5) are the real and imaginary parts of electric potential $\phi(\boldsymbol{x},\omega)$, the solution of (2.6), (2.7).

Variational principles (3.3)–(3.5) have been used extensively in the analysis and the numerical solution of both forward and inverse problems. In this survey, we review their use in studies of high-contrast materials (see section 5) and in numerical reconstructions of $\gamma(\boldsymbol{x},\omega)$ (see section 7.2.2).

The mathematical formulation of EIT, as first posed by Calderón [33], is as follows.

Definition 1. *Find the $L^\infty(\overline{\Omega})$ admittivity function $\gamma(\boldsymbol{x},\omega)$, with strictly positive real part $\sigma(\boldsymbol{x})$, given the DtN map Λ_γ.*

In practice, it is not advisable to work with the DtN map. Instead, one uses the NtD map $(\Lambda_\gamma)^{-1}$ which, as shown below, is smoothing and therefore better behaved for noisy measurements. Nevertheless, in theory, both maps contain the same information and, usually, the DtN map is used for convenience.

The NtD map $(\Lambda_\gamma)^{-1}: \mathcal{J} \to H^{\frac{1}{2}}(\partial\Omega)$ is defined on the restricted space of currents

$$\mathcal{J} = \left\{ I(\boldsymbol{x},\omega) \in H^{-\frac{1}{2}}(\partial\Omega) \text{ such that } \int_{\partial\Omega} I(\boldsymbol{x},\omega)\,\mathrm{d}s(\boldsymbol{x}) = 0 \right\} \tag{3.6}$$

and, for any $I(\boldsymbol{x},\omega) \in \mathcal{J}$, $(\Lambda_\gamma)^{-1} I(\boldsymbol{x},\omega) = \phi(\boldsymbol{x},\omega)$ at $\partial\Omega$, where $\phi(\boldsymbol{x},\omega)$ is the solution of Neumann boundary value problem (2.6), (2.8), (2.9). For $\omega = 0$, we have that $(\Lambda_\gamma)^{-1} \equiv (\Lambda_\sigma)^{-1}$ satisfies the following lemma.

Lemma 3. *The NtD map $(\Lambda_\sigma)^{-1}$ is self-adjoint and positive definite, with variational formulation*

$$\langle I, (\Lambda_\sigma)^{-1} I\rangle = \min_{\substack{\nabla\cdot\boldsymbol{j}=0 \\ -\boldsymbol{j}\cdot\boldsymbol{n}|_{\partial\Omega}=I}} \int_\Omega \frac{1}{\sigma(\boldsymbol{x})} |\boldsymbol{j}(\boldsymbol{x})|^2\,\mathrm{d}\boldsymbol{x}, \qquad \text{for arbitrary } I(\boldsymbol{x}) \in \mathcal{J}. \tag{3.7}$$

That $(\Lambda_\sigma)^{-1}$ is self-adjoint and positive definite follows easily from integration by parts, in a calculation similar to (3.2). The Thompson variational principle (3.7) is proved in [44].

When $\omega \neq 0$, we find, similar to lemma 2, that $(\Lambda_\gamma)^{-1}$ is complex symmetric but not self-adjoint. Furthermore, the real and imaginary parts of quadratic forms $\langle I^\star, (\Lambda_\gamma)^{-1} I\rangle$ have saddle point variational principles, similar to (3.4) and (3.5) (see [40, 67]).

Independent of the frequency ω, we note that $(\Lambda_\gamma)^{-1}$ is the generalized inverse of Λ_γ. More explicitly, the quadratic forms of the DtN and NtD maps are related by duality relations, which we give below for the dc problem.

Lemma 4. *In the static case $\omega = 0$, we have the convex duality relations*

$$\langle V, \Lambda_\sigma V\rangle = \sup_{I\in\mathcal{J}} \{2\langle I, V\rangle - \langle I, (\Lambda_\sigma)^{-1} I\rangle\}, \qquad \text{for any } V(\boldsymbol{x}) \in H^{\frac{1}{2}}(\partial\Omega), \tag{3.8}$$

$$\langle I, (\Lambda_\sigma)^{-1} I\rangle = \sup_{V\in H^{\frac{1}{2}}(\partial\Omega)} \{2\langle I, V\rangle - \langle V, \Lambda_\sigma V\rangle\}, \qquad \text{for any } I(\boldsymbol{x}) \in \mathcal{J}. \tag{3.9}$$

The proof of lemma 4 can be found, for example, in [64]. Duality relations for the complex problem $\omega \neq 0$ can be found in [40, 67].

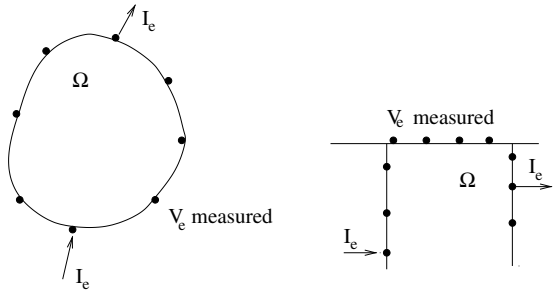

Figure 1. Illustration of experimental setups for gathering partial data about the DtN map.

3.2. Imaging with incomplete, noisy data

In practice, we do not have full knowledge of maps $(\Lambda_\gamma)^{-1}$ or Λ_γ, respectively. Instead, we have a set of N *experiments*, where we define an excitation pattern $I_e(\boldsymbol{x}, \omega) \in \mathcal{J}$ and we measure the resulting voltage $V_e(\boldsymbol{x}_p, \omega)$, at discrete locations $\boldsymbol{x}_p \in \partial\Omega$ of the electrodes, along the boundary. In figure 1, we illustrate two experimental setups. Excitation current I_e is injected (extracted) at some electrodes and the resulting voltage is measured at all or some of the electrodes. The first setup is typical of medical applications, where one has access at all points of the boundary. The second setup is typical of geophysics applications, where measurements can be made at the earth's surface or in some boreholes. In any case, we say that we have *partial* knowledge of the NtD map and, furthermore, the data V_e are usually contaminated with noise. The practical EIT problem is the following.

Definition 2. *Find admittivity function $\gamma(\boldsymbol{x}, \omega)$, given partial, noisy knowledge of $(\Lambda_\gamma)^{-1}$.*

All theoretical results reviewed in this paper assume full knowledge of the DtN (NtD) maps (see definition 1). However, most numerical reconstructions use the more realistic definition 2 of EIT.

4. Uniqueness of solutions

In this section, we address the identifiability question: given the boundary measurements, can we uniquely determine $\gamma(\boldsymbol{x}, \omega)$ in $\overline{\Omega}$?

In some important applications, such as nondestructive testing, the unknown γ can be restricted to a special class of functions. For example, we can suppose that $\gamma(\boldsymbol{x}, \omega)$ takes two known values γ_1 or γ_2, for $\boldsymbol{x}$ inside or outside an unknown, possibly multiple-connected subdomain D of Ω. Then, it is possible to identify γ with less than full knowledge of the DtN map (see for example [92, 93] and the references within).

We assume here full knowledge of Λ_γ, as was done initially by Calderón in his influential paper [33], and we review some of the important results on the injectivity of the DtN map, for a large class of functions γ. We begin with the identifiability of γ at $\partial\Omega$ (section 4.1), after which we address the uniqueness of solutions in the interior of Ω (sections 4.2, 4.3). In section 4.4, we discuss the anisotropic problem, where γ is tensor valued. Finally, we consider the EIT problem for discrete resistor networks in section 4.5.

4.1. Uniqueness and continuous dependence at the boundary

The first proof of unique identifiability of σ and its normal derivatives at the boundary, by the DtN map Λ_σ, has been obtained by Kohn and Vogelius [105], under the assumptions that Ω is a bounded, C^∞ domain, and σ is an $L^\infty(\overline{\Omega})$, strictly positive function, which is C^∞ in a neighbourhood of $\partial\Omega$. To prove uniqueness at an arbitrary $\boldsymbol{x}_0 \in \partial\Omega$, they used energy estimates and carefully designed boundary data $V \in H^{\frac{1}{2}}(\partial\Omega)$, which are highly oscillatory and vanish outside a small neighbourhood of $\boldsymbol{x}_0$. Such boundary conditions ensure that the solution of (2.6), (2.7) decays rapidly away from $\boldsymbol{x}_0$, and is thus suitable for determining σ at this point.

By using techniques of microlocal analysis, Sylvester and Uhlmann [145] give explicit reconstruction formulae for σ and its normal derivatives at $\partial\Omega$, under the assumptions that Ω is bounded and C^∞, and $\sigma \in C^\infty(\overline{\Omega})$, such that Λ_σ is a pseudodifferential operator of order 1 (see [32]). Take $\boldsymbol{x}$ in the vicinity of $\boldsymbol{x}_0 \in \partial\Omega$ and let $\boldsymbol{x} - \boldsymbol{x}_0 = (\boldsymbol{z}', z_n)$, where $\boldsymbol{z}' \in \mathbb{R}^{n-1}$ and $z_n = 0$ for $\boldsymbol{x} \in \partial\Omega$. The symbol of Λ_σ is given by (see [145])

$$\Lambda_\sigma(\boldsymbol{z}', \boldsymbol{\xi}') = \sigma(\boldsymbol{z}', 0)|\boldsymbol{\xi}'| + a(\boldsymbol{z}', \boldsymbol{\xi}') + r(\boldsymbol{z}', \boldsymbol{\xi}'), \tag{4.1}$$

where $a(\boldsymbol{z}', \boldsymbol{\xi}')$ is homogeneous of degree 0 in $\boldsymbol{\xi}'$ and it is determined by the normal and tangential first derivatives of σ, at $(\boldsymbol{z}', 0)$. Term $r(\boldsymbol{z}', \boldsymbol{\xi}')$ in (4.1) is a classical symbol of order -1 and it is determined by higher order normal and tangential derivatives of σ, at $(\boldsymbol{z}', 0)$. Then, from the definition of symbol Λ_σ and (4.1), the boundary reconstruction is

$$\sigma(\boldsymbol{z}', 0) = \lim_{|\boldsymbol{\xi}'|\to\infty} \frac{\mathrm{e}^{-\mathrm{i}\boldsymbol{z}'\cdot\boldsymbol{\xi}'}}{|\boldsymbol{\xi}'|} \Lambda_\sigma \mathrm{e}^{\mathrm{i}\boldsymbol{z}'\cdot\boldsymbol{\xi}'}. \tag{4.2}$$

Normal derivatives of σ, at $\partial\Omega$, can be determined inductively. For example, the first normal derivative $\partial\sigma(\boldsymbol{z}', 0)/\partial n$ is given by the principal symbol of map $\Lambda_\sigma - \sigma|_{\partial\Omega}\Lambda_1$, where $\sigma|_{\partial\Omega}$ denotes the trace of σ at the boundary and Λ_1 is the DtN map for a constant conductivity, equal to 1.

Boundary reconstructions are also given by Nachman [117]. His technique does not require that Λ_σ be a pseudodifferential operator and, as a result, the previous assumptions are relaxed to a $C^{1,1}$ boundary $\partial\Omega$, and conductivity $\sigma \in C^{1,1}(\overline{\Omega})$. Nachman's formulae for conductivity σ and its normal derivative at $\partial\Omega$ are

$$\lim_{|\boldsymbol{k}|\to\infty} \|2\mathrm{e}^{-\mathrm{i}\boldsymbol{x}\cdot\boldsymbol{k}} S_0 \Lambda_\sigma \mathrm{e}^{\mathrm{i}\boldsymbol{x}\cdot\boldsymbol{k}} - \sigma(\boldsymbol{x})\|_{L^2(\partial\Omega)} = 0 \tag{4.3}$$

and

$$\lim_{|\boldsymbol{k}|\to\infty} \left\| \mathrm{e}^{-\mathrm{i}\boldsymbol{x}\cdot\boldsymbol{k}} (\sigma\Lambda_1 + \Lambda_1\sigma - 2\Lambda_\sigma) \mathrm{e}^{\mathrm{i}\boldsymbol{x}\cdot\boldsymbol{k}} - \frac{\partial\sigma}{\partial n} \right\|_{L^2(\partial\Omega)} = 0, \tag{4.4}$$

respectively, where S_0 is the single layer potential operator $S_0 f(\boldsymbol{x}) = \int_{\partial\Omega} G_0(\boldsymbol{x}, \boldsymbol{y}) f(\boldsymbol{y})\, \mathrm{d}s$ and G_0 is the free space Green function for the Laplace equation.

Explicit reconstructions such as (4.2), have been used further by Sylvester and Uhlmann [145, 148] in proving stability estimates:

Theorem 1. *Suppose that σ_1 and σ_2 are two bounded, strictly positive and continuous functions. The trace of $\sigma_1 - \sigma_2$ at $\partial\Omega$ (assumed smooth) can be bounded in terms of the operator norm of $\Lambda_{\sigma_1} - \Lambda_{\sigma_2}$, from $H^{\frac{1}{2}}(\partial\Omega)$ to $H^{-\frac{1}{2}}(\partial\Omega)$, as*

$$\|\sigma_1 - \sigma_2\|_{L^\infty(\partial\Omega)} \leqslant C \|\Lambda_{\sigma_1} - \Lambda_{\sigma_2}\|_{H^{\frac{1}{2}}(\partial\Omega), H^{-\frac{1}{2}}(\partial\Omega)}, \tag{4.5}$$

where C is a constant depending on Ω and dimension d.

The proof of (4.5) is given in [145]. It is also shown there that, if σ_1 and σ_2 are Lipschitz continuous, $\left\| \frac{\partial \sigma_1}{\partial n} - \frac{\partial \sigma_2}{\partial n} \right\|_{L^\infty(\partial\Omega)}$ is bounded in terms of $\|\Lambda_{\sigma_1} - \Lambda_{\sigma_2}\|_{H^{\frac{1}{2}}(\partial\Omega), H^{-\frac{1}{2}}(\partial\Omega)}$, as well.

Note in particular that the stability estimates derived in [145] imply uniqueness of a Lipschitz-continuous conductivity and its normal derivative at $\partial\Omega$, as follows. Take a $C^\infty(\overline{\Omega})$ function σ_1 in (4.5) and let σ_2 be its Lipschitz continuous approximation. Then, $\|\Lambda_{\sigma_1} - \Lambda_{\sigma_2}\|_{H^{\frac{1}{2}}(\partial\Omega), H^{-\frac{1}{2}}(\partial\Omega)}$ is bounded in terms of the approximation error $\|\sigma_1 - \sigma_2\|_{L^\infty(\Omega)}$ (see [145]). Since σ_1 and $\frac{\partial \sigma_1}{\partial n}$ are uniquely determined at $\partial\Omega$ by Λ_{σ_1} (see [105]), the uniqueness of the Lipschitz conductivity at $\partial\Omega$ follows from stability estimate (4.5). Similarly, uniqueness of the normal boundary derivative of a Lipschitz conductivity function follows from the stability bound on $\|\frac{\partial \sigma_1}{\partial n} - \frac{\partial \sigma_2}{\partial n}\|_{L^\infty(\partial\Omega)}$, given in [145].

We conclude with the observation that explicit reconstruction formulae in the interior of Ω are not possible, in general, but uniqueness still holds, as shown next.

4.2. Uniqueness in the interior. The linearized problem

The EIT problem was first posed by Calderón, in the fundamental paper [33]. He considered the static case $\omega = 0$, where Dirichlet variational principle (3.3) applies, but his results extend to the complex case $\omega \neq 0$, as well. Let us polarize the quadratic form (3.3) and obtain

$$Q_\sigma(V, W) = \langle W, \Lambda_\sigma V \rangle = \int_\Omega \sigma(\boldsymbol{x}) \nabla\phi(\boldsymbol{x}) \cdot \nabla\psi(\boldsymbol{x}) \, \mathrm{d}\boldsymbol{x}, \tag{4.6}$$

where ϕ and ψ are solutions of (2.6), (2.7), for $\omega = 0$ (i.e. $\gamma = \sigma$) and Dirichlet data V and W, respectively. Recall that Λ_σ is self-adjoint and note that $Q_\sigma(V, W)$, for all V and W in $H^{\frac{1}{2}}(\partial\Omega)$, determines Λ_σ, itself.

Calderón proved that map Q_σ is analytic and that its Fréchet derivative at $\sigma = \sigma^0(\boldsymbol{x})$, in direction $h(\boldsymbol{x})$, is

$$DQ_{\sigma^0}(V, W)h = \int_\Omega h(\boldsymbol{x}) \nabla\phi^0(\boldsymbol{x}) \cdot \nabla\psi^0(\boldsymbol{x}) \, \mathrm{d}\boldsymbol{x}, \tag{4.7}$$

where ϕ^0 and $\psi^0 \in H^1(\Omega)$ are solutions of

$$\begin{aligned} &\nabla \cdot [\sigma^0(\boldsymbol{x}) \nabla\phi^0(\boldsymbol{x})] = \nabla \cdot [\sigma^0(\boldsymbol{x}) \nabla\psi^0(\boldsymbol{x})] = 0 \qquad \text{in } \Omega \\ &\phi^0(\boldsymbol{x}) = V(\boldsymbol{x}), \\ &\psi^0(\boldsymbol{x}) = W(\boldsymbol{x}) \qquad \text{at } \partial\Omega. \end{aligned} \tag{4.8}$$

Then, the linearized map is injective, if the products $\nabla\phi^0 \cdot \nabla\psi^0$ are dense in $L^2(\Omega)$.

Calderón considered linearization at a constant, say $\sigma^0 = 1$, and he assumed that $h(\boldsymbol{x})$ vanishes near $\partial\Omega$. To prove injectivity of the linearized map $Q_1 + DQ_1 h$, he supposed that

$$\int_\Omega h(\boldsymbol{x}) \nabla\phi^0(\boldsymbol{x}) \cdot \nabla\psi^0(\boldsymbol{x}) \, \mathrm{d}\boldsymbol{x} = 0, \tag{4.9}$$

for all harmonic functions ϕ^0, ψ^0, in Ω. In particular, he chose harmonic functions

$$\phi^0(\boldsymbol{x}) = \mathrm{e}^{\boldsymbol{x} \cdot \boldsymbol{\xi}}, \qquad \psi^0(\boldsymbol{x}) = \mathrm{e}^{-\boldsymbol{x} \cdot \boldsymbol{\xi}^\star}, \tag{4.10}$$

where

$$\boldsymbol{\xi} = \boldsymbol{\rho} + \frac{\mathrm{i}}{2}\boldsymbol{k}, \qquad \text{for } \boldsymbol{\rho}, \boldsymbol{k} \in \mathbb{R}^d, \text{ such that } |\boldsymbol{\rho}| = \frac{|\boldsymbol{k}|}{2} \text{ and } \boldsymbol{\rho} \cdot \boldsymbol{k} = 0. \tag{4.11}$$

Then, using (4.10) in (4.9) and extending $h(\boldsymbol{x})$ to 0 outside domain Ω,

$$|\boldsymbol{\xi}|^2 \int_\Omega h(\boldsymbol{x}) \mathrm{e}^{\boldsymbol{x} \cdot (\boldsymbol{\xi} - \boldsymbol{\xi}^\star)} \, \mathrm{d}\boldsymbol{x} = \frac{|\boldsymbol{k}|^2}{2} \int_{\mathbb{R}^d} h(\boldsymbol{x}) \mathrm{e}^{\mathrm{i}\boldsymbol{k} \cdot \boldsymbol{x}} \, \mathrm{d}\boldsymbol{x} = \frac{|\boldsymbol{k}|^2}{2} \hat{h}(\boldsymbol{k}) = 0, \qquad \text{for all } \boldsymbol{k} \in \mathbb{R}^d, \tag{4.12}$$

such that, by the Fourier inversion formula, $h(\boldsymbol{x}) = 0$ everywhere in $\mathbb{R}^d$. Equivalently, the linearized map at constant σ^0 is injective.

Complex exponentials (4.10) are of great importance in the theoretical study of nonlinear EIT (see section 4.3) and they allow an explicit reconstruction of $h(\boldsymbol{x})$, as follows [33]: let us suppose that the perturbation of σ is small, of order $\delta \ll 1$, and rescale h as $h \to \delta h$, such that $\sigma(\boldsymbol{x}) = 1 + \delta h(\boldsymbol{x})$ in Ω. Consider $V(\boldsymbol{x}) = \mathrm{e}^{\boldsymbol{x}\cdot\boldsymbol{\xi}}$, $W(\boldsymbol{x}) = \mathrm{e}^{-\boldsymbol{x}\cdot\boldsymbol{\xi}^\star}$ for $\boldsymbol{x} \in \partial\Omega$, the boundary traces of harmonic functions (4.10). Calderón showed that

$$\|\nabla(\phi - \phi^0)\|_{L^2(\Omega)} \leqslant \delta C \|h(\boldsymbol{x})\|_{L^\infty(\Omega)}, \qquad \|\nabla(\psi - \psi^0)\|_{L^2(\Omega)} \leqslant \delta C \|h(\boldsymbol{x})\|_{L^\infty(\Omega)},$$

for some constant C, and he obtained

$$\delta\hat{h}(\boldsymbol{k}) = -\frac{2}{|\boldsymbol{k}|^2}\left[Q_\sigma(\mathrm{e}^{\boldsymbol{x}\cdot\boldsymbol{\xi}}, \mathrm{e}^{-\boldsymbol{x}\cdot\boldsymbol{\xi}^\star}) - \int_{\partial\Omega} \boldsymbol{\xi}\cdot\boldsymbol{n}(\boldsymbol{x})\mathrm{e}^{\mathrm{i}\boldsymbol{k}\cdot\boldsymbol{x}}\,\mathrm{d}s(\boldsymbol{x}) \right] + \mathrm{O}(\delta^2) \qquad \text{for any } \boldsymbol{k} \neq 0. \tag{4.13}$$

The accuracy of Calderón's reconstruction (4.13) has been tested in [91], for Ω a unit disc and

$$\delta h(\boldsymbol{x}) = \begin{cases} a & \text{if } |\boldsymbol{x}| \leqslant r < 1, \\ 0 & \text{elsewhere.} \end{cases}$$

In this example, $\delta h(\boldsymbol{x}) \approx \frac{2a}{2+a}\sum_{p=0}^{\infty}\left(-\frac{a}{2+a}\right)^p \chi_{r^{p+1}}(\boldsymbol{x})$ (see [91]), where $\chi_{r^{p+1}}$ is the characteristic function of a disc of radius r^{p+1}, concentric with Ω. As expected, the reconstruction is accurate if $a \ll 1$. For larger a, (4.13) gives an infinite number of jump discontinuities of the reconstructed $\delta h(\boldsymbol{x})$, with only the first discontinuity occurring at correct radius r.

4.3. Uniqueness in the interior. The nonlinear problem

Even though the analytic map Q_σ has an injective Fréchet derivative at constant σ^0 (see section 4.2 and [33]), the inverse of DQ_{σ^0} is unbounded and we cannot apply the implicit function theorem. In particular, the injectivity of DQ_{σ^0} does not imply the injectivity of nonlinear map Q_σ, even for σ near a constant.

One of the first uniqueness results for nonlinear EIT is given by Kohn and Vogelius, for analytic σ, as an immediate corollary to their boundary identification result (see [105] and section 4.1). The extension to piecewise analytic conductivities, in C^∞ subdomains of analyticity, is done in [107].

Uniqueness of piecewise constant σ, with piecewise smooth interfaces of discontinuity, in a domain Ω which can be unbounded, is given by Druskin [58]. The extension to piecewise analytic σ is given in [59]. Druskin's approach is based on the theory of the Cauchy problem for elliptic second-order partial differential equations and it exploits heavily the properties of Green functions near the discontinuities of σ. Note that Druskin's results address inverse problems encountered in geophysics, where one does not have measurements everywhere around $\partial\Omega$. For example, he shows that in three dimensions, measurements of $\Lambda_\sigma V$ in an arbitrary two-dimensional subset of $\partial\Omega$, guarantee uniqueness of σ in Ω.

The question of injectivity of the nonlinear Λ_γ map, in dimensions $d \geqslant 3$, is answered, for a large class of functions γ, by Sylvester and Uhlmann, in [144]. Their proof is extended to a reconstruction algorithm, by Nachman [117]. In two dimensions, the injectivity of the dc map Λ_σ is established by Nachman [118], in a constructive proof which has been implemented in [134]. We review these fundamental results in sections 4.3.1–4.3.3.

4.3.1. Complex geometrical optics for Schrödinger's equation. Uniqueness in dimensions $d \geqslant 3$. Sylvester and Uhlmann [144] discovered that complex exponentials (4.10) can also be used for variable functions γ, in the high-frequency limit $|\boldsymbol{\xi}| \to \infty$, where WKB-type estimates of the potential inside Ω hold. Their fundamental uniqueness result is the following.

Theorem 2. *Let* $\Omega \subset \mathbb{R}^d$, $d \geqslant 3$, *be a bounded, simply connected domain with* C^∞ *boundary. Suppose that* γ_1 *and* γ_2 *are* $C^\infty(\overline{\Omega})$ *functions with strictly positive real parts. If* $\Lambda_{\gamma_1} V = \Lambda_{\gamma_2} V$, *for all* $V \in H^{\frac{1}{2}}(\partial\Omega)$, $\gamma_1 = \gamma_2$ *in* $\overline{\Omega}$.

Before describing Sylvester and Uhlmann's proof of theorem 2, let us note the following extensions: in [116, 117], uniqueness is proved for a $C^{1,1}$ boundary and function $\gamma \in C^{1,1}(\overline{\Omega})$. Further extensions were obtained by Brown [29] for $W^{\frac{3}{2}+\delta}(\overline{\Omega})$, $\delta > 0$, conductivities and by Päivärinta *et al* [122] for Lipschitz conductivities. Note that the latter is the strongest known uniqueness result, for dimension $d \geqslant 3$.

In [144], Sylvester and Uhlmann begin their proof of theorem 2, by transforming the EIT problem into an inverse scattering problem for Schrödinger's equation

$$\Delta u(\boldsymbol{x}, \omega) - q(\boldsymbol{x}, \omega) u(\boldsymbol{x}, \omega) = 0, \tag{4.14}$$

where Δ is the Laplace operator,

$$u(\boldsymbol{x}, \omega) = \gamma^{\frac{1}{2}}(\boldsymbol{x}, \omega)\phi(\boldsymbol{x}, \omega) \qquad \text{and} \qquad q(\boldsymbol{x}, \omega) = \frac{\Delta \gamma^{\frac{1}{2}}(\boldsymbol{x}, \omega)}{\gamma^{\frac{1}{2}}(\boldsymbol{x}, \omega)} \quad \text{in } \Omega. \tag{4.15}$$

The inverse scattering problem is: *Find scattering potential* $q(\boldsymbol{x}, \omega) \in L^\infty(\overline{\Omega})$, *given* $\Gamma_q f(\boldsymbol{x}, \omega) = \frac{\partial u(\boldsymbol{x}, \omega)}{\partial n}$ *for* $\boldsymbol{x} \in \partial\Omega$ *and arbitrary Dirichlet data* $u|_{\partial\Omega} = f \in H^{\frac{1}{2}}(\partial\Omega)$. Note that Γ_q is given in terms of Λ_γ as

$$\Gamma_q f(\boldsymbol{x}, \omega) = \frac{1}{2}\gamma^{-1}(\boldsymbol{x}, \omega)\frac{\partial \gamma(\boldsymbol{x}, \omega)}{\partial n} f(\boldsymbol{x}, \omega) + \gamma^{-\frac{1}{2}}(\boldsymbol{x}, \omega)\Lambda_\gamma(\gamma^{-\frac{1}{2}} f)(\boldsymbol{x}, \omega) \qquad \text{for } \boldsymbol{x} \in \partial\Omega \tag{4.16}$$

and, since γ and its normal derivative are uniquely determined at $\partial\Omega$ (see section 4.1), the inverse scattering problem and the EIT problem are equivalent, for sufficiently smooth γ.

To obtain the injectivity of Γ_q, Sylvester and Uhlmann show first that (4.14) admits complex geometrical optics solutions

$$u(\boldsymbol{x}, \omega) = u(\boldsymbol{x}, \omega; \boldsymbol{\xi}) = \mathrm{e}^{\mathrm{i}\boldsymbol{x}\cdot\boldsymbol{\xi}}(1 + \psi(\boldsymbol{x}, \omega; \boldsymbol{\xi})), \qquad \boldsymbol{\xi} \in \mathbb{C}^d \text{ such that } \boldsymbol{\xi} \cdot \boldsymbol{\xi} = 0, \tag{4.17}$$

where

$$\nabla\psi(\boldsymbol{x}, \omega; \boldsymbol{\xi}) + 2\mathrm{i}\boldsymbol{\xi} \cdot \nabla\psi(\boldsymbol{x}, \omega; \boldsymbol{\xi}) - q(\boldsymbol{x}, \omega)\psi(\boldsymbol{x}, \omega; \boldsymbol{\xi}) = q(\boldsymbol{x}, \omega) \qquad \text{in } \Omega \tag{4.18}$$

and $\|\psi\|^2_{L^2_\delta(\Omega)} = \int_\Omega (1+|\boldsymbol{x}|^2)^\delta |\psi(\boldsymbol{x}, \omega; \boldsymbol{\xi})|^2 \, \mathrm{d}\boldsymbol{x}$ decays like $1/|\boldsymbol{\xi}|^2$, for $-1 < \delta < 0$ and $|\boldsymbol{\xi}| \gg 1$.

Now, suppose that q_1 and q_2 are two scattering potentials, satisfying $\Gamma_{q_1} = \Gamma_{q_2}$. Due to the uniqueness of γ and its derivatives at the boundary, $\delta q(\boldsymbol{x}, \omega) = q_1(\boldsymbol{x}, \omega) - q_2(\boldsymbol{x}, \omega)$ vanishes at $\partial\Omega$ and, by integration by parts,

$$\int_\Omega \delta q(\boldsymbol{x}, \omega) u_1(\boldsymbol{x}, \omega) u_2(\boldsymbol{x}, \omega) \, \mathrm{d}\boldsymbol{x} = 0, \tag{4.19}$$

where u_1, u_2 are solutions of (4.14), for the same boundary data and scattering potentials q_1 and q_2, respectively. Following Calderón's approach, Sylvester and Uhlmann take

$$u_j(\boldsymbol{x}, \omega) = u(\boldsymbol{x}, \omega; \boldsymbol{\xi}_j) = \mathrm{e}^{\mathrm{i}\boldsymbol{x}\cdot\boldsymbol{\xi}_j}(1 + \psi(\boldsymbol{x}, \omega; \boldsymbol{\xi}_j)), \qquad j = 1, 2, \tag{4.20}$$

for $\boldsymbol{\xi}_1, \boldsymbol{\xi}_2 \in \mathbb{C}^d$, $\boldsymbol{\xi}_1 \cdot \boldsymbol{\xi}_1 = \boldsymbol{\xi}_2 \cdot \boldsymbol{\xi}_2 = 0$ and $\boldsymbol{\xi}_1 + \boldsymbol{\xi}_2 = \boldsymbol{k}$, a fixed, arbitrary vector in $\mathbb{R}^d$. In particular, they let $|\boldsymbol{\xi}_1|$ and $|\boldsymbol{\xi}_2| \to \infty$, such that

$$\int_\Omega \delta q(\boldsymbol{x}, \omega) \mathrm{e}^{\mathrm{i}\boldsymbol{x}\cdot\boldsymbol{k}} \,\mathrm{d}\boldsymbol{x} = \int_\Omega \delta q(\boldsymbol{x}, \omega) \mathrm{e}^{\mathrm{i}\boldsymbol{x}\cdot\boldsymbol{k}} [\psi(\boldsymbol{x}, \omega; \boldsymbol{\xi}_1) + \psi(\boldsymbol{x}, \omega; \boldsymbol{\xi}_2) + \psi_1(\boldsymbol{x}, \omega; \boldsymbol{\xi}_1)\psi_2(\boldsymbol{x}, \omega; \boldsymbol{\xi}_2)] \,\mathrm{d}\boldsymbol{x} \to 0$$

and, by setting $\delta q = 0$ outside Ω, they obtain $\delta\hat{q}(\boldsymbol{k}, \omega) = 0$ for all $\boldsymbol{k} \in \mathbb{R}^d$. Finally, by the Fourier inversion formula, the scattering potential $q(\boldsymbol{x}, \omega)$ is uniquely determined by Γ_q and the admittivity γ is the unique solution of the Dirichlet boundary value problem

$$\begin{aligned} &\Delta\gamma^{\frac{1}{2}}(\boldsymbol{x}, \omega) - \gamma^{\frac{1}{2}}(\boldsymbol{x}, \omega) q(\boldsymbol{x}, \omega) = 0 \qquad \text{in } \Omega \\ &\gamma^{\frac{1}{2}}(\boldsymbol{x}, \omega) = \text{given at } \partial\Omega. \end{aligned} \tag{4.21}$$

Even though most ingredients of Sylvester and Uhlmann's proof of theorem 2 hold in any dimension, the construction of the high-frequency complex vectors $\boldsymbol{\xi}_1$ and $\boldsymbol{\xi}_2$, as needed in (4.20), can be done only in $\mathbb{C}^d$, for $d \geqslant 3$. Uniqueness in two dimensions is proved by Nachman [118], who also uses complex exponentials but does not rely on the high-frequency limit, as we discuss in section 4.3.3.

4.3.2. Reconstructing the conductivity in dimensions $d \geqslant 3$. The complex exponential solutions (4.17) have also been used by Nachman [117] for reconstructing $\sigma \in C^{1,1}(\overline{\Omega})$, given the map Λ_σ at the $C^{1,1}$ boundary $\partial\Omega$.

Nachman's algorithm begins with the inverse scattering problem for Schrödinger's equation (4.14). At $\partial\Omega$, σ and $\partial\sigma/\partial n$ are given by (4.3), (4.4), and the map Γ_q follows from (4.16). Inside Ω, $\sigma(\boldsymbol{x})$ can be calculated in terms of the scattering potential $q(\boldsymbol{x})$, by solving boundary value problem (4.21). Hence, the problem reduces to finding the scattering potential $q(\boldsymbol{x})$ from Γ_q.

Suppose that $q(\boldsymbol{x})$ is compactly supported in Ω and consider the *scattering transform* of q,

$$t(\boldsymbol{k}, \boldsymbol{\xi}) = \int_\Omega q(\boldsymbol{x}) u(\boldsymbol{x}; \boldsymbol{\xi}) \mathrm{e}^{-\mathrm{i}\boldsymbol{x}\cdot(\boldsymbol{k}+\boldsymbol{\xi})} \,\mathrm{d}\boldsymbol{x} = \int_{\mathbb{R}^d} q(\boldsymbol{x}) \mathrm{e}^{-\mathrm{i}\boldsymbol{x}\cdot\boldsymbol{k}} [1 + \psi(\boldsymbol{x}; \boldsymbol{\xi})] \,\mathrm{d}\boldsymbol{x}, \tag{4.22}$$

where $u(\boldsymbol{x}; \boldsymbol{\xi})$ are the geometrical optics solutions (4.17) (for $\omega = 0$) and $\boldsymbol{k} \in \mathbb{R}^d$. Nachman requires that both $\mathrm{e}^{-\mathrm{i}\boldsymbol{x}\cdot(\boldsymbol{k}+\boldsymbol{\xi})}$ and $\mathrm{e}^{-\mathrm{i}\boldsymbol{x}\cdot\boldsymbol{\xi}}$ be harmonic functions, so $(\boldsymbol{k}+\boldsymbol{\xi}) \cdot (\boldsymbol{k}+\boldsymbol{\xi}) = \boldsymbol{\xi} \cdot \boldsymbol{\xi} = 0$. For example, for any $\lambda > 0$, we can take $\boldsymbol{\xi} = -\boldsymbol{k}/2 + \boldsymbol{a} + \mathrm{i}\boldsymbol{b}$, where $\boldsymbol{a}$, $\boldsymbol{b}$ and $\boldsymbol{k}$ are orthogonal in $\mathbb{R}^d$ and $|\boldsymbol{a}| = \lambda$, $|\boldsymbol{b}| = \sqrt{\lambda^2 + |\boldsymbol{k}|^2/4}$, and we obtain the Fourier coefficients of q, in the limit $\lambda \to \infty$ (i.e. $|\boldsymbol{\xi}| \to \infty$), as

$$\hat{q}(-\boldsymbol{k}) = \lim_{|\boldsymbol{\xi}|\to\infty} t(\boldsymbol{k}, \boldsymbol{\xi}) \qquad \text{for any } \boldsymbol{k} \in \mathbb{R}^d. \tag{4.23}$$

The remaining question is, how to find the scattering transform $t(\boldsymbol{k}, \boldsymbol{\xi})$ from Γ_q?

Using (4.14) in (4.22), recalling that $\mathrm{e}^{-\mathrm{i}\boldsymbol{x}\cdot(\boldsymbol{k}+\boldsymbol{\xi})}$ is harmonic and integrating by parts, we have

$$\begin{aligned} t(\boldsymbol{k}, \boldsymbol{\xi}) &= \int_\Omega \mathrm{e}^{-\mathrm{i}\boldsymbol{x}\cdot(\boldsymbol{k}+\boldsymbol{\xi})} \Delta u(\boldsymbol{x}; \boldsymbol{\xi}) \,\mathrm{d}\boldsymbol{x} = \int_{\partial\Omega} [\mathrm{e}^{-\mathrm{i}\boldsymbol{x}\cdot(\boldsymbol{k}+\boldsymbol{\xi})} \Gamma_q u(\boldsymbol{x}; \boldsymbol{\xi}) - u(\boldsymbol{x}; \boldsymbol{\xi}) \Gamma_0 \mathrm{e}^{-\mathrm{i}\boldsymbol{x}\cdot(\boldsymbol{k}+\boldsymbol{\xi})}] \,\mathrm{d}s(\boldsymbol{x}) \\ &= \int_{\partial\Omega} \mathrm{e}^{-\mathrm{i}\boldsymbol{x}\cdot(\boldsymbol{k}+\boldsymbol{\xi})} (\Gamma_q - \Gamma_0) u(\boldsymbol{x}; \boldsymbol{\xi}) \,\mathrm{d}s(\boldsymbol{x}), \end{aligned} \tag{4.24}$$

where Γ_0 is the DtN map of Laplace's equation. Note, however, that only the leading term of $u(\boldsymbol{x}; \boldsymbol{\xi})$ at $\partial\Omega$ is known. The amplitude $\psi(\boldsymbol{x}; \boldsymbol{\xi})$ must be calculated, and we cannot simply solve (4.18), because q is not known. Instead, Nachman finds ψ at $\partial\Omega$ by solving the exterior problem

$$\Delta u(\boldsymbol{x}; \boldsymbol{\xi}) = 0 \qquad \text{in } \mathbb{R}^d \setminus \overline{\Omega}, \qquad \frac{\partial u(\boldsymbol{x}; \boldsymbol{\xi})}{\partial n} = \Gamma_q u(\boldsymbol{x}; \boldsymbol{\xi}) \qquad \text{at } \partial\Omega \tag{4.25}$$

and, as $|\boldsymbol{x}| \to \infty$, $w(\boldsymbol{x};\boldsymbol{\xi}) = u(\boldsymbol{x};\boldsymbol{\xi}) - \mathrm{e}^{\mathrm{i}\boldsymbol{x}\cdot\boldsymbol{\xi}}$ satisfies the radiation condition

$$\lim_{R\to\infty}\int_{|\boldsymbol{x}|=R}\left[G_\xi(\boldsymbol{y},\boldsymbol{x})\frac{\partial w(\boldsymbol{x};\boldsymbol{\xi})}{\partial n} - w(\boldsymbol{x};\boldsymbol{\xi})\frac{\partial G_\xi(\boldsymbol{y},\boldsymbol{x})}{\partial n}\right]\mathrm{d}s(\boldsymbol{x}) = 0 \qquad \text{for almost all } \boldsymbol{y}, \tag{4.26}$$

where

$$G_\xi(\boldsymbol{y},\boldsymbol{x}) = \frac{\mathrm{e}^{\mathrm{i}(\boldsymbol{y}-\boldsymbol{x})\cdot\boldsymbol{\xi}}}{(2\pi)^d}\int_{\mathbb{R}^d}\frac{\mathrm{e}^{\mathrm{i}(\boldsymbol{y}-\boldsymbol{x})\cdot\boldsymbol{\zeta}}}{|\boldsymbol{\zeta}|^2 + 2\boldsymbol{\zeta}\cdot\boldsymbol{\xi}}\,\mathrm{d}\boldsymbol{\zeta} \tag{4.27}$$

is the Fadeev Green function of Laplace's equation. Nachman shows that $f(\boldsymbol{x};\boldsymbol{\xi}) = u|_{\partial\Omega}$ satisfies the integral equation of Fredholm type

$$f(\boldsymbol{x};\boldsymbol{\xi}) = \mathrm{e}^{\mathrm{i}\boldsymbol{x}\cdot\boldsymbol{\xi}} - (S_\xi\Gamma_q - B_\xi - \tfrac{1}{2}I)f(\boldsymbol{x};\boldsymbol{\xi}), \tag{4.28}$$

where $S_\xi f(\boldsymbol{x};\boldsymbol{\xi}) = \int_{\partial\Omega} G_\xi(\boldsymbol{x},\boldsymbol{y})f(\boldsymbol{y};\boldsymbol{\xi})\,\mathrm{d}s(\boldsymbol{y})$, $B_\xi f(\boldsymbol{x};\boldsymbol{\xi}) = \text{p.v.}\int_{\partial\Omega}\frac{\partial G_\xi(\boldsymbol{x},\boldsymbol{y})}{\partial n}f(\boldsymbol{y};\boldsymbol{\xi})\,\mathrm{d}s(\boldsymbol{y})$, are single- and double-layer potentials, respectively. He also proves that the integral operator $\frac{1}{2}I + S_\xi\Gamma_q - B_\xi$ is invertible and, moreover, (4.28) has a unique solution $f(\boldsymbol{x};\boldsymbol{\xi}) = u|_{\partial\Omega}$, which belongs to $H^{3/2}(\partial\Omega)$.

The reconstruction process is completed by using the calculated $u(\boldsymbol{x};\boldsymbol{\xi})$ at $\partial\Omega$ in (4.24), taking the limit (4.23) and finally, solving (4.21) for σ. Note that Nachman gives an alternative to formula (4.23), for q in terms of t, as well. Nevertheless, both formulae require high complex frequencies and they should be unstable in practice, due to exponential amplification of noise in Γ_q.

4.3.3. Uniqueness in two dimensions. Local uniqueness in two dimensions has been obtained for conductivities $\sigma \in W^{3,\infty}(\overline{\Omega})$, which are approximately constant, by Sylvester and Uhlmann [143]. Further, Sun and Uhlmann [140] show that the space $W^{3,\infty}(\overline{\Omega})$ of conductivities contains an open dense set $\mathcal{O}$ such that, if σ_1 and σ_2 are close to an element in $\mathcal{O}$, $\Lambda_{\sigma_1} = \Lambda_{\sigma_2}$ implies $\sigma_1 = \sigma_2$. Other results, for quite special functions σ, are given by Sun [138, 139] and Sylvester [142]. However, the global two-dimensional uniqueness problem has been solved by Nachman [118], in his fundamental theorem, as follows.

Theorem 3. *Let Ω be a bounded, Lipschitz domain in $\mathbb{R}^2$ and take two positive conductivity functions $\sigma_1, \sigma_2 \in W^{2,p}(\Omega)$, for $p > 1$. If $\Lambda_{\sigma_1} = \Lambda_{\sigma_2}$, then $\sigma_1 = \sigma_2$.*

The first steps in Nachman's proof of theorem 3 have already been described in section 4.3.2. The EIT problem is transformed into the inverse scattering problem for Schrödinger's equation, the scattering transform $t(\boldsymbol{k};\boldsymbol{\xi})$ is given in terms of Γ_q by equation (4.24), and the trace of $u(\boldsymbol{x};\boldsymbol{\xi})$ at $\partial\Omega$ is calculated by solving (4.28). However, q cannot be extracted from t by taking the high-frequency limit, since in two dimensions, there is not enough freedom to have $\boldsymbol{\xi}\cdot\boldsymbol{\xi} = (\boldsymbol{\xi}+\boldsymbol{k})\cdot(\boldsymbol{\xi}+\boldsymbol{k}) = 0$ for arbitrary $\boldsymbol{k} \in \mathbb{R}^2$, and $|\boldsymbol{\xi}| \to \infty$, at the same time. Instead, Nachman's proof proceeds as follows.

Let $\boldsymbol{\xi} = (\zeta, \mathrm{i}\zeta) \in \mathbb{C}^2$, where $\zeta \in \mathbb{C}$, $\boldsymbol{k} = -2\,\mathrm{Re}\{\boldsymbol{\xi}\}$, such that $(\boldsymbol{k}+\boldsymbol{\xi})\cdot(\boldsymbol{k}+\boldsymbol{\xi}) = \boldsymbol{\xi}^\star\cdot\boldsymbol{\xi}^\star = \boldsymbol{\xi}\cdot\boldsymbol{\xi} = 0$, and define

$$\mu(\boldsymbol{x};\boldsymbol{\xi}) = \mathrm{e}^{-\mathrm{i}\boldsymbol{x}\cdot\boldsymbol{\xi}}u(\boldsymbol{x};\boldsymbol{\xi}) = 1 + \psi(\boldsymbol{x};\boldsymbol{\xi}). \tag{4.29}$$

In terms of the new variable ζ and $z = x_1 + \mathrm{i}x_2$, the scattering transform becomes

$$t(\zeta) \equiv t(-2\,\mathrm{Re}\{\boldsymbol{\xi}\},\boldsymbol{\xi}) = \int_\Omega q(\boldsymbol{x})\mu(\boldsymbol{x};\zeta)\mathrm{e}^{\mathrm{i}(\overline{\zeta}\,\overline{z}+\zeta z)}\,\mathrm{d}\boldsymbol{x} = \int_{\partial\Omega}\mathrm{e}^{\mathrm{i}\overline{\zeta}\,\overline{z}}(\Gamma_q - \Gamma_0)\mathrm{e}^{\mathrm{i}\zeta z}\mu(\boldsymbol{x};\zeta)\,\mathrm{d}s(\boldsymbol{x}). \tag{4.30}$$

Nachman proves that $\mu(\boldsymbol{x};\zeta)$ is the unique solution of the $\overline{\partial}$ equation

$$\frac{\partial \mu(\boldsymbol{x};\zeta)}{\partial \overline{\zeta}} = \frac{1}{4\pi\overline{\zeta}}\, t(\zeta) \mathrm{e}^{-(\overline{\zeta}\,\overline{z}+\zeta z)} \overline{\mu(\boldsymbol{x};\zeta)}, \tag{4.31}$$

or, equivalently, of the integral equation

$$\mu(\boldsymbol{x};\zeta) = 1 + \frac{1}{4\pi^2}\int_{\mathbb{R}^2} \frac{t(\zeta')}{\overline{\zeta'}(\zeta'-\zeta)} \mathrm{e}^{-\mathrm{i}(\overline{\zeta'}\,\overline{z}+\zeta' z)} \overline{\mu(\boldsymbol{x};\zeta')}\, \mathrm{d}\zeta'_{\mathrm{R}}\, \mathrm{d}\zeta'_{\mathrm{I}}, \qquad \text{where } \zeta' = \zeta'_{\mathrm{R}} + \mathrm{i}\zeta'_{\mathrm{I}}. \tag{4.32}$$

At low frequency $\zeta \ll 1$, the scattering transform is $|t(\zeta)| = \mathrm{O}(|\zeta|^2)$ and the trace of u at $\partial\Omega$ can be estimated from (4.28) as $\|u(\boldsymbol{x};\zeta) - 1\|_{H^{\frac{1}{2}}(\partial\Omega)} = \mathrm{O}(|\zeta|)$ [118, 134]. Finally, recalling that $\sigma^{-1/2}u$ solves the EIT equations, using the maximum principle and regularity and embedding theorems, Nachman obtains

$$\sigma^{\frac{1}{2}}(\boldsymbol{x}) = \lim_{\zeta\to 0}\mu(\boldsymbol{x};\zeta) = 1 + \frac{1}{4\pi^2}\int_{\mathbb{R}^2} \frac{t(\zeta')}{|\zeta'|^2} \mathrm{e}^{-\mathrm{i}(\overline{\zeta'}\,\overline{z}+\zeta' z)} \overline{\mu(\boldsymbol{x};\zeta')}\, \mathrm{d}\zeta'_{\mathrm{R}}\, \mathrm{d}\zeta'_{\mathrm{I}} \qquad \text{for all } \boldsymbol{x}\in\Omega. \tag{4.33}$$

Nachman's proof has been successfully implemented and tested by Siltanen *et al* [134]. Theorem 3 has also been extended by Brown and Uhlmann [30] to less regular conductivities $\sigma \in W^{1,p}$, for $p > 1$. Uniqueness for even less regular σ is not known.

Note that all the results reviewed in this section apply to the static problem, whereas uniqueness in three or more dimensions is known for complex admittivities, as well (see section 4.3.1 and [144, 148]). While the complex problem is not entirely solved in two dimensions, substantial progress has been made by Francini [69], who proves the unique identification of complex $\gamma \in W^{1,\infty}(\Omega)$, by Λ_γ, if $\mathrm{Im}\{\gamma\}$ is sufficiently small (i.e. ω is small).

4.4. Anisotropic materials

The electrical properties of anisotropic materials depend on direction and the admittivity γ is a complex-symmetric, matrix-valued function, with positive definite real part. Unfortunately, the DtN map for anisotropic γ is not injective, as shown by a simple calculation in [106]: let $\Psi : \overline{\Omega} \to \overline{\Omega}$ be any smooth diffeomorphism, which is the identity at $\partial\Omega$. Let $D\Psi$ be the differential of Ψ and $D\Psi^T$ its transpose. Then, $\Lambda_{\tilde{\gamma}} = \Lambda_\gamma$, where $\tilde{\gamma}$ is the transformed admittivity γ through Ψ,

$$\tilde{\gamma}(\boldsymbol{x},\omega) = \frac{(D\Psi^T \gamma D\Psi)\circ\Psi^{-1}}{|\det(D\Psi|)}(\boldsymbol{x},\omega). \tag{4.34}$$

Since uniqueness does not hold for anisotropic EIT, we rephrase the question as: *does the DtN map Λ_γ determine γ, up to a diffeomorphism Ψ?* The answer is affirmative for real-valued $\gamma = \sigma$, in two dimensions, if $\sigma \in C^{2,\alpha}(\overline{\Omega})$, $0 < \alpha < 1$ and $\partial\Omega$ is $C^{3,\alpha}$ (see [141][1]) and in three dimensions, if σ is analytic [111] (see also [146, 148, 149]).

4.5. Electrical networks

Networks arise in many applications, by themselves, or as modelling tools for creeping, ground water flow [109], flow in high-contrast media [27, 75, 81], etc. Electrical conduction through

[1] In [141], the authors use isothermal coordinates (available only in two dimensions) to show that the anisotropic problem reduces to an isotropic one. Then, uniqueness follows from Nachmann's proof [118].

networks is described by Kirchhoff's circuit laws and it is well understood. In this section, we consider the inverse problem: *find the electrical network which has a given DtN map*.

A network $(\mathcal{N}, \mathcal{B}, \gamma)$ consists of sets $\mathcal{N}$ and $\mathcal{B}$ of nodes and branches (edges), respectively. An edge $(p, k) \in \mathcal{B}$ connects two nodes $p, k \in \mathcal{N}$ and it has an admittivity $\gamma_{p,k}$. Suppose that there are N_b boundary nodes in $\mathcal{N}$. The network DtN map, $\Lambda_\gamma^{\text{net}}$, is the complex-symmetric $N_b \times N_b$ matrix, which takes the vector $\boldsymbol{\mathcal{V}} = (\mathcal{V}_1, \ldots, \mathcal{V}_{N_b})^T$ of boundary voltages and maps it into the vector $\boldsymbol{\mathcal{I}} = (\mathcal{I}_1, \ldots, \mathcal{I}_{N_b})^T$ of boundary electric currents. The NtD map $(\Lambda_\gamma^{\text{net}})^{-1}$ is the generalized inverse of the DtN map and it is defined on the restricted set of currents which satisfy $\sum_{p=1}^{N_b} \mathcal{I}_p = 0$. As in the continuum, the quadratic forms of $\Lambda_\gamma^{\text{net}}$ and $(\Lambda_\gamma^{\text{net}})^{-1}$ have variational formulations and they are related by duality relations (see for example [27, 28]).

It is easy to see that the injectivity of the DtN map $\Lambda_\gamma^{\text{net}}$ does not hold, in general. Nevertheless, there are special situations, of fixed and known network topology, where the network is uniquely determined by $\Lambda_\gamma^{\text{net}}$. This is the case of planar, rectangular networks, where each interior node has four neighbours, and each boundary node is connected to just one node, belonging to $\mathcal{N} \setminus \mathcal{N}_b$. Uniqueness for such networks has been established by Curtis and Morrow [46] and by Grünbaum and Zubelli [76][2]. They independently developed the same constructive proof of injectivity of $\Lambda_\gamma^{\text{net}}$, which recovers the network in a layer peeling fashion, marching from the boundary, towards the interior of the domain. This algorithm is very appealing because of its simplicity and it has been implemented by many. Unfortunately, it is extremely ill-conditioned and it does not work, in practice, for larger than 10×10 rectangular networks.

Another example of identifiable network is the circular planar ones considered by Curtis *et al* [45] (see also [86]) and, independently, by Colin de Verdière [47, 48].

Nevertheless, the injectivity question for more general networks remains open. In particular, the necessary and sufficient conditions that a network should satisfy in order to be identifiable from the DtN map are not known, so far.

5. High-contrast EIT

In some applications, such as geophysics, electrical properties of materials can have *high contrast*. For example, a dry rock matrix is insulating compared with liquid-filled pores, some pore liquids, such as hydrocarbons, are poor conductors in comparison with other pore liquids, such as brines, and so on. The fact is that the subsurface electrical conductivity can vary over several orders of magnitude in Ω, even at macroscopic length scales, where some averaging is already built into the model.

Clearly, there are many ways in which high contrast can arise in a medium. We concentrate here on materials with dense arrays of highly conducting or insulating inclusions, in a smooth background. Such high-contrast materials are at or near the percolation threshold (inclusions are close to touching), and they pose difficult theoretical and computational challenges in both forward and inverse problems. In particular, the injectivity results of section 4 do not apply.

Electrical conduction in high-contrast materials, with periodic or random structure, has been studied from the homogenization point of view in [12, 16, 27, 100, 101, 110]. However, these works do not address the issue of boundary conditions, which is key in inversion. The first

[2] Note that [76] considers a simplified model for isotropic diffusion tomography, with equations similar to Kirchhoff's laws for rectangular resistor networks. In particular, instead of an unknown resistor R_{ij} of a branch connecting nodes i and j in the network, the equations in [76] contain w_{ij}, the probability that a photon is not absorbed at a pixel location (i, j) in a planar domain. Nevertheless, the proposed reconstruction of w_{ij} is basically the same as that in [46], for finding resistors R_{ij}.

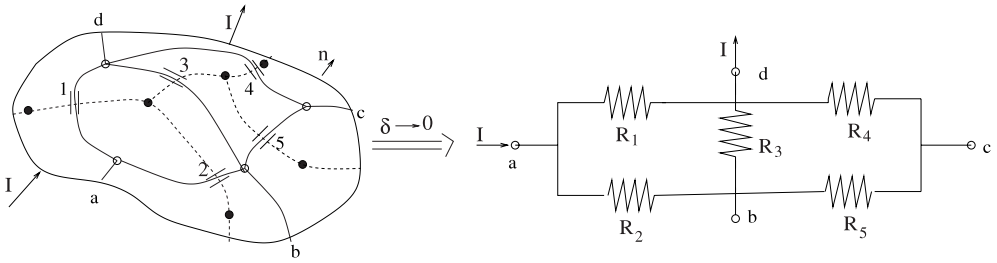

Figure 2. Example of an asymptotically equivalent resistor network.

characterization of the DtN map of high-contrast materials has been obtained by Borcea, Berryman and Papanicolaou in [24] (see also [21, 23, 27, 28]), in two dimensions. Their results extend to some three-dimensional problems, as well, but the general case is not yet understood. We review in this section the static high-contrast problem considered in [23, 24]. For the complex admittivity problem, we refer the reader to [27, 28].

Since in most applications, detailed information about the medium, such as the shape of inclusions, is lacking, the high-contrast conductivity is modelled in [24] as a continuous function

$$\sigma(\boldsymbol{x}) \equiv \sigma_\delta(\boldsymbol{x}) = \sigma^0 \mathrm{e}^{-S(\boldsymbol{x})/\delta}, \tag{5.1}$$

where σ^0 is constant, $S(\boldsymbol{x})$ is a smooth function with isolated, nondegenerate critical points (a Morse function) and δ is a small but positive parameter, such that the contrast of σ_δ is exponentially large (see also [110]). It is shown in [24] that, in the limit $\delta \to 0$, Λ_{σ_δ} is asymptotically equivalent to the DtN map of a resistor network. Discrete network approximations of continuum conduction problems have been considered in the past, as finite-difference discretizations of the differential equations [46, 51]. However, the asymptotic networks considered in [24] are radically different. They arise because of strong channelling of electric currents in high-contrast materials, they are uniquely defined by conductivity σ_δ and they are rigorously justified by the analysis in [24].

The flow channelling in high-contrast media can be understood from the asymptotic analysis of equations (2.10), as follows: for σ given by (5.1), we have the singularly perturbed problem

$$\nabla \times \boldsymbol{j}(\boldsymbol{x}) + \frac{1}{\delta} \nabla S(\boldsymbol{x}) \times \boldsymbol{j}(\boldsymbol{x}) = 0 \qquad \text{in } \Omega \tag{5.2}$$

and, as $\delta \to 0$, $\boldsymbol{j}$ flows in the direction of ∇S, along the paths (ridges) of maximal conductivity [27, 110]. When the contrast is high, $\boldsymbol{j}$ is strongly concentrated and it flows like current in a network. Along the ridges of maximal conductivity, there are maxima and saddle points of σ_δ, where $\nabla S = 0$. A local asymptotic analysis near these points reveals that $\nabla\phi = -\boldsymbol{j}/\sigma$ is very small near maxima of σ_δ and very large at its saddle points [27, 110]. The maxima of σ_δ are then the nodes of the network and the edges connect adjacent maxima through the saddles $\boldsymbol{x}_s$, where the energy is dissipated just as in a resistor $R = \frac{1}{\sigma(\boldsymbol{x}_s)}\sqrt{\frac{k_+}{k_-}}$, where k_+ and k_- are the curvatures of S at $\boldsymbol{x}_s$.

In figure 2 we illustrate the construction of the asymptotic resistor network. We take a continuum with a high-contrast σ_δ that has four maxima and six minima shown in the figure by $\circ$ and $\bullet$, respectively. There are also five saddle points of σ_δ denoted in the figure by $1, \ldots, 5$. The current avoids the minima of σ_δ and it is attracted by its maxima. Each maximum of σ_δ has a basin of attraction delimited in Ω by the ridge of minimal conductivity passing through

the neighbouring saddle points (see dotted curves in figure 2). Because of the external driving, the current flows from one maximum of σ_δ to another, along the least resistive paths (see solid lines in figure 2), like current in a resistor network. The branches of the network connect adjacent maxima of σ_δ through the saddle points. In figure 2 we have five branches, each one carrying a resistance $R_i, i = 1, \ldots, 5$. Finally, the peripheral nodes a, b, c and d are the points of intersection of the ridges of maximal conductivity with the boundary.

Let then $\Lambda^{\text{net}}_{\sigma_\delta}$, $(\Lambda^{\text{net}}_{\sigma_\delta})^{-1}$ be the DtN and NtD maps of the asymptotic network, which is uniquely determined for any high-contrast conductivity (5.1), as shown above. In the limit $\delta \to 0$, we have the following theorem.

Theorem 4. *For any current $I(\boldsymbol{x}) \in H^{-\frac{1}{2}}(\partial\Omega)$ such that $\int_{\partial\Omega} I(\boldsymbol{x})\,\mathrm{d}s = 0$,*

$$\langle I, (\Lambda_{\sigma_\delta})^{-1} I\rangle = \boldsymbol{\mathcal{I}}^T (\Lambda^{\text{net}}_{\sigma_\delta})^{-1} \boldsymbol{\mathcal{I}}[1 + \mathrm{o}(1)], \tag{5.3}$$

where $\boldsymbol{\mathcal{I}} = (\mathcal{I}_1, \ldots \mathcal{I}_{\mathrm{N}_b})^T$, $\mathcal{I}_p = \int_{\partial\Omega \bigcap \overline{B}(\boldsymbol{x}_p)} I(\boldsymbol{x})\,\mathrm{d}s$ and $\overline{B}(\boldsymbol{x}_p)$ is the closure of the basin of attraction of the maximum of σ_δ associated with the pth boundary node. Furthermore, for any potential $V(\boldsymbol{x}) \in H^{\frac{1}{2}}(\partial\Omega)$,

$$\langle V, \Lambda_{\sigma_\delta} V\rangle = \boldsymbol{\mathcal{V}}^T \Lambda^{\text{net}}_{\sigma_\delta} \boldsymbol{\mathcal{V}}[1 + \mathrm{o}(1)], \tag{5.4}$$

where $\boldsymbol{\mathcal{V}} = (\mathcal{V}_1, \ldots, \mathcal{V}_{\mathrm{N}_b})^T$, $\mathcal{V}_p = V(s_p)$ and s_p is the intersection of $\partial\Omega$ with the ridge of maximal σ_δ, associated with boundary node p.

The proof of theorem 4 is given in [24] and it relies on variational principles (3.3), (3.7). Explicitly, carefully designed test functions ϕ and $\boldsymbol{j}$ are used in (3.3), (3.7), to get tight upper bounds on $\langle V, \Lambda_{\sigma_\delta} V\rangle$ and $\langle I, (\Lambda_{\sigma_\delta})^{-1} I\rangle$, respectively. The lower bounds are given by duality relations (3.9). In the asymptotic limit $\delta \to 0$, the lower and upper bounds match and they are given by the quadratic forms $\boldsymbol{\mathcal{V}}^T \Lambda^{\text{net}}_{\sigma_\delta} \boldsymbol{\mathcal{V}}$ and $\boldsymbol{\mathcal{I}}^T (\Lambda^{\text{net}}_{\sigma_\delta})^{-1} \boldsymbol{\mathcal{I}}$ for the asymptotic network, respectively.

In conclusion, high-contrast EIT reduces to imaging the asymptotic network. Unfortunately, as explained in section 4.5, there may be many networks that have the same DtN maps and the high-contrast EIT problem does not have, in general, a unique solution. Equivalently, even though the high-contrast σ_δ given by (5.1) leads to a *unique* asymptotic network, there may be infinitely many functions σ_δ that match the boundary measurements. Then, inversion cannot be done, unless some additional constraints are imposed on σ_δ. For example, in [23, 24], the authors reconstruct the 'smallest' network which matches the data, with a matching pursuit approach, where the network elements are found one at a time.

6. Instability of EIT

Without *a priori* restrictions on the class of admittivities γ, the inverse map $\Lambda_\gamma \to \gamma$, taken from $[H^{\frac{1}{2}}(\partial\Omega), H^{-\frac{1}{2}}(\partial\Omega)]$ to $L^\infty(\Omega)$, is discontinuous and the EIT problem is severely ill-posed. A heuristic argument for the instability of EIT is that, to find γ, we need the potential ϕ inside the domain. However, ϕ satisfies an elliptic equation with Cauchy data $\phi|_{\partial\Omega} = V$ and $\sigma\,\partial\phi/\partial n|_{\partial\Omega} = \Lambda_\gamma V$, which is ill-posed, as given by Hadamard [80], so the EIT problem is ill-posed, as well.

A simple example of instability of EIT is given by Alessandrini [2], for Ω the unit disc and a conductivity function

$$\sigma(\boldsymbol{x}) = \begin{cases} 1 + a & \text{if } |\boldsymbol{x}| \leqslant r < 1, \\ 1 & \text{elsewhere,} \end{cases} \tag{6.1}$$

where $a > -1$ is a bounded constant. For any voltage $V(\theta) = \sum_{n=-\infty}^{\infty} V_n e^{in\theta}$ in $H^{\frac{1}{2}}(\partial\Omega)$, the DtN maps for conductivity (6.1) and $\sigma \equiv 1$ are

$$\Lambda_\sigma V(\theta) = \sum_{n=-\infty}^{\infty} |n| V_n \frac{2 + a(1 + r^{2|n|})}{2 + a(1 - r^{2|n|})} e^{in\theta}, \qquad \Lambda_1 V(\theta) = \sum_{n=-\infty}^{\infty} |n| V_n e^{in\theta},$$

respectively. Since $\|\sigma - 1\|_{L^\infty(\Omega)} = |a|$, independently of r, while $\lim_{r\to 0}(\Lambda_\sigma - \Lambda_1)V(\theta) = 0$, for all $\theta \in [0, 2\pi)$, the inverse map is discontinuous.

In numerical computations, it is very expensive to work with fractional-order Sobolev spaces and the inverse map is usually taken from $[L^2(\partial\Omega), L^2(\partial\Omega)]$ to $L^\infty(\Omega)$, or $L^2(\Omega)$. In this case, a typical example of instability comes from the theory of homogenization, where the conductivity $\sigma(\boldsymbol{x}, \boldsymbol{x}/\delta) \equiv \sigma_\delta(\boldsymbol{x})$ oscillates at the very small scale $\delta \ll 1$. A common homogenization result is that, as $\delta \to 0$, the electric potential ϕ_δ, corresponding to σ_δ, converges weakly in $H^1(\Omega)$ to $\overline{\phi}(\boldsymbol{x})$, the potential for the smooth, effective (homogenized) conductivity $\overline{\sigma}(\boldsymbol{x})$ (see for example [13]). Then, by the compact trace embedding, $\lim_{\delta\to 0} \|\phi_\delta - \overline{\phi}\|_{L^2(\partial\Omega)} = \lim_{\delta\to 0} \|(\Lambda_{\sigma_\delta})^{-1} I - (\Lambda_{\overline{\sigma}})^{-1} I\|_{L^2(\partial\Omega)} = 0$, for $I \in L^2(\partial\Omega)$, even though σ_δ and $\overline{\sigma}$ are very different functions.

6.1. Stability estimates

In order to have stability of EIT, it is required that some constraints be placed on σ (or γ, if $\omega \neq 0$). For example, Alessandrini [2] gives the following logarithmic stability estimate:

$$\|\sigma_1 - \sigma_2\|_{L^\infty(\Omega)} \leqslant C \log\Big(\|\Lambda_{\sigma_1} - \Lambda_{\sigma_2}\|_{H^{\frac{1}{2}}(\partial\Omega), H^{-\frac{1}{2}}(\partial\Omega)}\Big)^{-\delta}, \qquad \delta \in (0, 1), \tag{6.2}$$

for $\sigma_1, \sigma_2 \in H^{2+s}(\Omega)$ and $s > d/2$. Logarithmic stability estimates have also been obtained for the inverse problem of crack detection by Alessandrini [3] and Alessandrini and Rondi [6]. Furthermore, in [4], Alessandrini shows that in corrosion detection by EIT, the logarithmic estimate is the best possible stability result.

6.2. Distinguishability, resolution and stabilization

An exact stability analysis of the EIT problem, linearized at a constant conductivity in a unit disc, is given by Allers and Santosa [7]. They reformulate linearized EIT as a moment problem, obtain an explicit reconstruction of the perturbation of σ and, finally, assess both the stability and the resolution limit of the image. The conclusion is that stability is achieved at the cost of loss in resolution, especially for points in the centre of the domain.

Since all measurements are noisy, it is important to understand the set of indistinguishable perturbations $\delta\sigma$, at noise level δ,

$$\mathcal{P}_\delta = \Big\{\delta\sigma \in L^\infty(\Omega) \text{ such that } \|(\Lambda_{\sigma^0+\delta\sigma})^{-1} - (\Lambda_{\sigma^0})^{-1}\|_{H^{-\frac{1}{2}}(\partial\Omega), H^{\frac{1}{2}}(\partial\Omega)} \leqslant \delta\Big\},$$

which is, for all practical purposes, the null space of $D(\Lambda_{\sigma^0})^{-1}$, the Fréchet derivative of the NtD map at σ^0. The concept of *distinguishability* has been introduced by Isaacson [88] and Seagar [133] and it has been studied extensively in the static ($\omega = 0$) case (see for example [38, 42, 52, 54]). Note however that, due to the difficulty of working with fractional-order Sobolev spaces, basically all studies consider the larger set

$$\Big\{\delta\sigma \in L^\infty(\Omega) \text{ such that } \|(\Lambda_{\sigma^0+\delta\sigma})^{-1} - (\Lambda_{\sigma^0})^{-1}\|_{L^2(\partial\Omega), L^2(\partial\Omega)} \leqslant \delta\Big\} \supseteq \mathcal{P}_\delta. \tag{6.3}$$

Note also that all the available characterizations of distinguishability rely on variational principle (3.7) and they do not extend to the complex admittivity problem, which is much less understood.

A very interesting characterization of the indistinguishable perturbations $\delta\sigma$ about constant $\sigma^0 = 1$ is given by Dobson [52, 54]. Following Calderón's approach, Dobson considers the polarized quadratic form $Q_{1+\delta\sigma}(I, J) = \langle I, (\Lambda_{1+\delta\sigma})^{-1} J\rangle$, for $I, J \in L^2(\partial\Omega)$, with linearization

$$DQ_1(I, J)\delta\sigma = -\int_\Omega \delta\sigma(\boldsymbol{x})\nabla\phi^0(\boldsymbol{x}) \cdot \nabla\psi^0(\boldsymbol{x})\,\mathrm{d}\boldsymbol{x}, \tag{6.4}$$

where ϕ^0 and ψ^0 are harmonic functions in Ω, satisfying boundary conditions $\partial\phi^0/\partial n|_{\partial\Omega} = I$ and $\partial\psi^0/\partial n|_{\partial\Omega} = J$, respectively. Then, he lets

$$\|DQ_1\delta\sigma\| = \sup_{\|I\|_{L^2(\Omega)}, \|J\|_{L^2(\Omega)} \leqslant 1} |DQ_1(I, J)\delta\sigma| \tag{6.5}$$

and finds two linear operators A and B, which are diagonal in some basis in $L^2(\Omega)$, such that

$$\|B\delta\sigma\| \leqslant \|DQ_1\delta\sigma\| \leqslant \|A\delta\sigma\|. \tag{6.6}$$

Consequently, if $\mathcal{U}_\delta$, $\mathcal{A}_\delta$ and $\mathcal{B}_\delta$ are the sets of perturbations $\delta\sigma$ satisfying $\|DQ_1\delta\sigma\| \leqslant \delta$, $\|A\delta\sigma\| \leqslant \delta$ and $\|B\delta\sigma\| \leqslant \delta$, respectively,

$$\mathcal{A}_\delta \subset \mathcal{U}_\delta \subset \mathcal{B}_\delta. \tag{6.7}$$

Dobson finds the lower bound in (6.6) with Calderón's method described in section 4.2: suppose that Ω is contained in a ball of radius R and take boundary currents

$$I(\boldsymbol{x}) = \alpha\nabla \mathrm{e}^{(\mathrm{i}\xi/2+\beta)\cdot\boldsymbol{x}} \cdot \boldsymbol{n}(\boldsymbol{x}), \qquad J(\boldsymbol{x}) = \alpha\nabla \mathrm{e}^{(\mathrm{i}\xi/2-\beta)\cdot\boldsymbol{x}} \cdot \boldsymbol{n}(\boldsymbol{x}) \qquad \text{at } \partial\Omega, \tag{6.8}$$

where $\boldsymbol{\xi}, \boldsymbol{\eta} \in \mathbb{R}^d$, $\boldsymbol{\xi}\cdot\boldsymbol{\eta} = 0$, $|\boldsymbol{\eta}| = |\boldsymbol{\xi}|/2$ and constant $\alpha = \sqrt{2\beta}\mathrm{e}^{-R|\xi|/2}$, $\beta = \mathrm{O}(1)$, is adjusted to get $\|I\|_{L^2(\partial\Omega)}, \|J\|_{L^2(\partial\Omega)} \leqslant 1$ (see [52, 54]). After an explicit calculation given in [52, 54], we have

$$\|DQ_1\delta\sigma\| \geqslant \sup_{\boldsymbol{\xi}\in\mathbb{R}^d} |DQ_1(I, J)\delta\sigma| = \sup_{\boldsymbol{\xi}\in\mathbb{R}^d} \beta|\boldsymbol{\xi}|^2\mathrm{e}^{-R|\xi|}\widehat{\delta\sigma}(\boldsymbol{\xi}) = \|B\delta\sigma\|. \tag{6.9}$$

Thus, the Fourier coefficients $\widehat{\delta\sigma}(\boldsymbol{\xi})$ appear to be determined with an exponentially increasing error in $\boldsymbol{\xi}$ and, to stabilize the reconstruction, we may be inclined to set $\widehat{\delta\sigma}(\boldsymbol{\xi}) = 0$, for large frequencies $\boldsymbol{\xi}$. However, the resulting image is typically too blurry to be of any interest and a better regularization approach is needed.

Dobson recalls from studies such as [7, 133] that the distinguishability near $\partial\Omega$ is much better than deep, in the interior of Ω. The pessimistic bound (6.9) makes no use of this fact and it treats all points $\boldsymbol{x} \in \Omega$ the same. A better alternative is given by a space-frequency analysis, which suggests discretizing conductivity σ in a wavelet basis. Indeed, Dobson proposes a wavelet construction of the upper-bound operator A in (6.6) and, he does some resolution analysis for Ω the unit disc and tensor products of Haar wavelets in $\mathbb{R}^2$. This idea is very promising but it has not been studied theoretically or numerically in a satisfactory manner, so far.

There is extensive literature on how to stabilize the inverse problem by some regularization approach, which ensures convergence of reconstruction algorithms, by restricting the admittivity γ to a compact subset of $L^\infty(\Omega)$. For example, we refer the reader to works [36, 65, 66, 82, 115, 147] and the references within and to the statistical, Bayesian approaches in [96, 97, 121]. Note, however, that basically all the known regularization methods make use of some '*a priori*' information about the unknown σ or γ and, as a result, they may introduce artifacts in the images. It is not clear yet which regularization method is better than the other and this area remains open for research.

7. Imaging methods

The numerical solution of the EIT problem has received increasing attention, lately, and many algorithms have been proposed, especially for the static problem ($\omega = 0$). We classify the imaging algorithms as iterative and noniterative and review some of them in sections 7.1 and 7.2. The nonlinear EIT problem is usually solved iteratively, by a sequence of linearizations at the guess of admittivity γ. This requires that the forward map be sufficiently smooth, as we discuss in section 7.2.4. The efficient calculation of derivatives of the objective function, via the adjoint method, is reviewed in section 7.2.5. The surveyed iterative methods are classified as output least squares (section 7.2.1) and variational (section 7.2.2) and they can be implemented on a single grid or on multigrids (section 7.3). Finally, the unknown γ can be discretized on an equidistant or better, on an adaptive (optimal) grid, as we discuss in section 7.4.

7.1. Noniterative algorithms

7.1.1. The linearized EIT problem A very ingenious reconstruction method for the linearized EIT problem around $\sigma^0 = 1$, in a unit disc Ω, is given by Barber and Brown in [11], and it is analysed by Santosa and Vogelius in [128] and by Berenstein and Tarabusi in [14]. We follow the exposition in [128]: Take a boundary excitation current $I = -\pi\,\partial\delta(\boldsymbol{x} - \boldsymbol{\xi})/\partial\tau$, the tangential derivative of the δ distribution (a dipole) at $\boldsymbol{\xi} = (\sin\beta, \cos\beta) \in \partial\Omega$ and solve (2.6), (2.8), for $\sigma = 1$, as

$$\phi^0(\boldsymbol{x}) \equiv u(\boldsymbol{x}, \boldsymbol{\xi}) = \frac{\boldsymbol{\xi}^\perp \cdot \boldsymbol{x}}{|\boldsymbol{\xi} - \boldsymbol{x}|^2}, \qquad \boldsymbol{\xi}^\perp = (-\cos\beta, \sin\beta). \tag{7.1}$$

Assuming a small perturbation $\delta\sigma$ of the conductivity, which vanishes at $\partial\Omega$, the perturbed potential is approximated by the solution of linearized equations

$$\Delta\delta u(\boldsymbol{x}, \boldsymbol{\xi}) = -\nabla\delta\sigma(\boldsymbol{x}) \cdot \nabla u(\boldsymbol{x}, \boldsymbol{\xi}) \qquad \text{in } \Omega, \qquad \frac{\partial\delta u(\boldsymbol{x}, \boldsymbol{\xi})}{\partial n} = 0 \qquad \text{at } \partial\Omega. \tag{7.2}$$

The change of coordinates from $\boldsymbol{x} = (x_1, x_2)$ to $(-u, v)$, where $v(\boldsymbol{x}, \boldsymbol{\xi}) = (1 - \boldsymbol{\xi}\cdot\boldsymbol{x})/|\boldsymbol{\xi} - \boldsymbol{x}|^2$ is the harmonic conjugate to $-u$ in Ω, maps conformally Ω into the upper half-space $\mathcal{H} = \{(-u, v), v \geqslant 1/2\}$. In particular, $\partial\Omega$ is mapped onto $\partial\mathcal{H} = \{(-u, v), v = 1/2\}$ and (7.2) becomes

$$\Delta\delta u = -\frac{\partial\delta\sigma}{\partial u} \qquad \text{in } \mathcal{H}, \qquad \frac{\partial\delta u}{\partial v} = 0 \qquad \text{at } \partial\mathcal{H}. \tag{7.3}$$

The perturbation $\delta\sigma$ would follow from (7.3) as $\delta\sigma(\boldsymbol{x}) = -\partial\delta u(u(\boldsymbol{x}, \boldsymbol{\xi}), v = 1/2)/\partial u$, except that it violates assumption $\delta\sigma|_{\partial\Omega} = 0$. Instead, $\delta\sigma$ is given by an average over the dipole locations [11, 128]

$$\delta\sigma(\boldsymbol{x}) \approx -\frac{1}{2\pi}\int_0^{2\pi} \mathrm{d}\alpha \left.\frac{\partial\delta u(\boldsymbol{x}^b(p, v = \frac{1}{2}), \boldsymbol{\xi})}{\partial u}\right|_{p=u(\boldsymbol{x},\boldsymbol{\xi})} \tag{7.4}$$

for any fixed, but arbitrary $\boldsymbol{x} \in \Omega$. Here, $\boldsymbol{x}^b$ is the intersection of $\partial\Omega$ with the equipotential line $p = u(\boldsymbol{x}, \boldsymbol{\xi})$ and α is the angle between the x_2 axis and the tangent to the equipotential line at $\boldsymbol{x}$ (see figure 3). Finally, as shown in [128],

$$\frac{\partial\delta u(\boldsymbol{x}^b(p, v = \frac{1}{2}), \boldsymbol{\xi})}{\partial u} = \frac{\frac{\partial\delta u}{\partial\tau}(\boldsymbol{x}^b(p, v = \frac{1}{2}), \boldsymbol{\xi})}{\frac{\partial u}{\partial\tau}|_{p=u(\boldsymbol{x},\boldsymbol{\xi})}} = \text{a measured quantity.}$$

In [128], Barber and Brown's backprojection algorithm is explained as an approximate inverse of Beylkin's generalized Radon transform [19] and it is used as a preconditioner in an

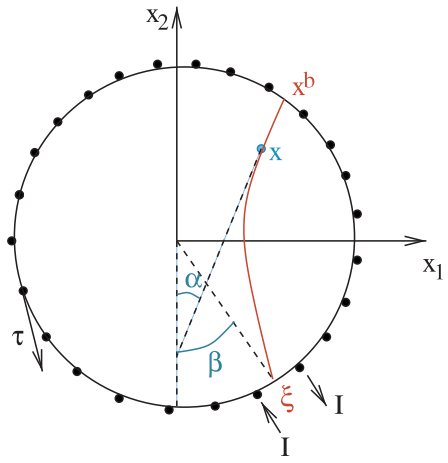

Figure 3. The dipole location is at $\boldsymbol{\xi} = (\sin\beta, \cos\beta)$ and the equipotential line $p = u(\boldsymbol{x}, \boldsymbol{\xi})$ through $\boldsymbol{x}$ intersects the boundary at $\boldsymbol{x}^b$.

iterative, conjugate residual method for the numerical solution of linearized EIT. Berenstein and Tarabusi [14] give a more precise characterization. They show that the linearized EIT problem in a unit disc can be interpreted *exactly* in terms of the Radon transform with respect to the Poincaré metric and a convolution operator. Barber and Brown's algorithm turns out to be a crude approximation of the exact representation in [14], which works best for smooth $\delta\sigma$ and for points near $\partial\Omega$. Finally, as expected, the inversion of the convolution operator in [14] is unstable and, so far, there is no known exact (or fully satisfactory) reconstruction of $\delta\sigma$ inside Ω.

7.1.2. The nonlinear EIT problem Layer stripping algorithms [46, 76, 136, 142] recover the unknown admittivity function γ, layer by layer, starting from $\partial\Omega$ and progressing inside Ω. Unfortunately, these algorithms are extremely unstable and, as such, they cannot be used for imaging, even for noiseless data, due to round-off errors. In general, it is not known how to stabilize the layer stripping approach, but there exists a stable algorithm, developed by Sylvester in [142], for one-dimensional EIT.

We conclude our survey of noniterative methods with those assuming a conductivity function

$$\sigma(\boldsymbol{x}) = \begin{cases} \sigma_j(\boldsymbol{x}) & \text{for } \boldsymbol{x} \in B_j \subset \Omega,\ j = 1, \dots M \\ 1 & \text{elsewhere,} \end{cases} \tag{7.5}$$

and seeking just the location of the interfaces ∂B_j of the inclusions contained in Ω. For example, in [31, 85], Brühl and Hanke image the inclusions B_j inside Ω as follows: let $G_{x_0,z}$ solve (in the sense of distributions) the differential equation

$$\Delta G_{x_0,z}(\boldsymbol{x}) = \Delta D_{x_0,z}(\boldsymbol{x}) \qquad \text{in } \Omega, \qquad \frac{\partial G_{x_0,z}(\boldsymbol{x})}{\partial n} = 0 \qquad \text{at } \partial\Omega, \tag{7.6}$$

where $\Delta D_{x_0,z}(\boldsymbol{x}) = 0$ for $\boldsymbol{x} \neq \boldsymbol{x}_0$ and $D_{x_0,z}(\boldsymbol{x}) = \frac{1}{2\pi}\frac{(\boldsymbol{x}-\boldsymbol{x}_0)\cdot\boldsymbol{z}}{|\boldsymbol{x}-\boldsymbol{x}_0|^d}$ is the dipole potential located at $\boldsymbol{x}_0 \in \mathbb{R}^d$. It is easy to see that the range of $(\Lambda_\sigma)^{-1} - (\Lambda_1)^{-1}$ consists of the trace at $\partial\Omega$ of harmonic functions in $\Omega \setminus \cup_{j=1}^m B_j$, with homogeneous Neumann boundary conditions at $\partial\Omega$ [31]. However, by (7.6), $G_{x_0,z}(\boldsymbol{x})|_{\partial\Omega}$ is precisely such a function, if $\boldsymbol{x}$ lies outside all

inclusions B_j, for $1 \leqslant j \leqslant M$. Then, Brühl and Hanke's algorithm searches for the inclusions, by testing with Picard's criterion, for each search point $\boldsymbol{x} \in \Omega$, if $G_{\boldsymbol{x}_0,z}(\boldsymbol{x})|_{\partial\Omega}$ belongs in the range of $(\Lambda_\sigma)^{-1} - (\Lambda_1)^{-1}$, or not.

Ikehata and Siltanen [85] give a similar algorithm. Note that [31, 85] are inspired by the ideas of Kirsch [103] for shape characterization of obstacles in inverse scattering. In fact, Kirsch's approach is quite similar to a well known signal processing method known as multiple signal classification (MUSIC) (see [50, 130]), as is pointed out by Cheney, in [37].

Finally, another very promising approach for locating interfaces of jump discontinuity of the conductivity σ is given by level set methods, as shown for example in [57, 94, 120, 126].

7.2. Iterative algorithms

It is convenient (but not really necessary) to assume in this section that admittivity γ is known at the boundary. This is commonly done in inversion and it is justified as follows: (1) in theory, $\gamma(\boldsymbol{x}, \omega)$ is uniquely and stably determined by the DtN or NtD maps (see section 4.1), (2) in practice, we have access at the boundary and γ can be measured there.

We define the set of admissible γ

$$\Upsilon = \{\gamma(\boldsymbol{x}, \omega) \in L^\infty(\overline{\Omega}) \text{ satisfying (2.5) and, for } \boldsymbol{x} \in \partial\Omega,\ \gamma(\boldsymbol{x}, \omega) = \text{known}\} \tag{7.7}$$

and we suppose that $\tilde{\gamma}$ is the admittivity function to be imaged, such that, for $I \in H^{-1/2}(\partial\Omega)$, the measured $V(\boldsymbol{x}, \omega) = (\Lambda_{\tilde{\gamma}})^{-1} I(\boldsymbol{x}, \omega)$ at $\partial\Omega$. Ideally, we would like to image $\gamma(\boldsymbol{x}, \omega)$ by minimizing the operator norm

$$\min_{\gamma\in\Upsilon} \left\| (\Lambda_\gamma)^{-1} - (\Lambda_{\tilde{\gamma}})^{-1} \right\|_{H^{-\frac{1}{2}}(\partial\Omega), H^{\frac{1}{2}}(\partial\Omega)}, \tag{7.8}$$

but, since only limited data are available (see section 3.2), we minimize instead

$$\min_{\gamma\in\Upsilon} \sum_{e=1}^{N} \left\| \left[(\Lambda_\gamma)^{-1} - (\Lambda_{\tilde{\gamma}})^{-1} \right] I_e \right\|^2_{H^{\frac{1}{2}}(\partial\Omega)}, \qquad \text{for } I_e \in H^{-1/2}(\partial\Omega),\ 1 \leqslant e \leqslant N. \tag{7.9}$$

Let us define the forward map $F : \Upsilon \times \mathcal{J} \to H^{\frac{1}{2}}(\partial\Omega)$, which is linear in I and nonlinear in γ, as

$$F[\gamma, I](\boldsymbol{x}, \omega) = (\Lambda_\gamma)^{-1} I(\boldsymbol{x}, \omega), \qquad \text{for } I(\boldsymbol{x}, \omega) \in \mathcal{J} \text{ and } \boldsymbol{x} \in \partial\Omega. \tag{7.10}$$

Assuming that $F[\gamma, I]$ is sufficiently smooth (see sections 7.2.4 and 7.2.5), nonlinear minimization problems such as (7.8) and (7.9) are solved iteratively, where, at step k, the estimated admittivity is $\gamma^{(k)}$ and $F[\gamma; I_e]$ is approximated by its best affine approximation near $\gamma^{(k)}$, for $k \geqslant 1$. Examples of such iterative algorithms can be found in [22, 51, 53, 79, 82, 108, 153] and the references within.

We review in sections 7.2.1 and 7.2.2, two classes of iterative, reconstruction methods:

(1) *Output least squares* methods which replace the operator norm in (7.8) with an approximation of the Hilbert–Schmidt norm over $L^2(\partial\Omega)$ and take the forward map as

$$F : \Upsilon \times \mathcal{J} \to L^2(\partial\Omega). \tag{7.11}$$

Working with the $L^2(\partial\Omega)$ norm, instead of $H^{1/2}(\partial\Omega)$, is motivated by the high cost of calculating fractional Sobolev space norms, as well as the possible lack of differentiability of the operator norm in (7.8). However, it is not really understood how this simplification affects the image, aside from some simple studies [38] which show that it can deteriorate the resolution.

(2) *Variational* methods, derived from variational principles (3.3) and (3.7), which are also known as *equation-error* approaches because at the 'solution', the potential ϕ which solves Dirichlet problem (2.6), (2.7) is related to current $\boldsymbol{j}$, the solution of (2.10), through Ohm's law (2.4). In particular, the minimization of (7.9), with the natural $H^{\frac{1}{2}}(\partial\Omega)$ norm, follows implicitly.

7.2.1. Output least squares It is shown in [52] that $(\Lambda_\gamma)^{-1} - (\Lambda_{\tilde{\gamma}})^{-1}$ is a Hilbert–Schmidt operator over $L^2(\partial\Omega)$, for a large class of admittivity functions. Let us then seek the solution $\tilde{\gamma}$ of the EIT problem as the minimizer of an approximation to the Hilbert–Schmidt norm

$$\left\|(\Lambda_\gamma)^{-1} - (\Lambda_{\tilde{\gamma}})\right\|_{HS}^2 \approx \sum_{e=1}^{N} \left\|\left[(\Lambda_\gamma)^{-1} - (\Lambda_{\tilde{\gamma}})^{-1}\right] I_e\right\|_{L^2(\partial\Omega)}^2, \tag{7.12}$$

for a set of N Neumann data $I_e \in \mathcal{J} \cap L^2(\partial\Omega)$, as is commonly done in numerical reconstructions. Since the EIT problem is ill-posed, convergence can only be ensured by means of some regularization technique. The output least-squares methods reconstruct γ (or just σ) by minimizing functional

$$\mathcal{R}(\gamma) = \sum_{e=1}^{N} \left\|\left[(\Lambda_\gamma)^{-1} - (\Lambda_{\tilde{\gamma}})^{-1}\right] I_e\right\|_{L^2(\partial\Omega)}^2 + \text{regularization term}, \tag{7.13}$$

over $\gamma \in \Upsilon$. The regularization term is usually of the form

$$\alpha \|B(\gamma - \gamma^0)\|_{L^2(\Omega)}^2, \tag{7.14}$$

where B is a linear operator (like the identity or gradient), γ^0 is a prior guess of γ and α is the regularization parameter. In the process of minimizing $\mathcal{R}(\gamma)$, γ^0 and α can be fixed or they can vary, the latter being referred to as iterative regularization. We direct the reader to [36, 65, 66, 82, 115, 147] for a detailed explanation of regularization techniques. We note that other choices, like total variation regularization [35], can also be made.

Basically, all nonlinear output least-squares algorithms [22, 51, 53, 82, 153] minimize $\mathcal{R}(\gamma)$ iteratively, with some Newton-type method [49]. The linearized output least-squares algorithms [7, 39] are particular cases of the nonlinear ones, where the 'solution' is accepted after the first iteration. Since the optimization methods require first and possibly second derivatives of the objective function, it is important to have an efficient way of calculating them. This is done by means of the adjoint method, as described in section 7.2.5.

There are two important questions that can affect the quality of the final image: (1) How to discretize the unknown γ? (2) What excitations I_e to choose? The first question is discussed in sections 7.3 and 7.4. The latter is addressed by Isaacson and collaborators in [38, 39, 72, 91], see also [42], for the static case ($\omega = 0$), as follows: suppose that we are interested in distinguishing σ from a given σ^0. Since

$$\left\|(\Lambda_\sigma)^{-1} - (\Lambda_{\sigma^0})\right\|_{HS}^2 = \sum_{e=1}^{\infty} \left\|\left[(\Lambda_\sigma)^{-1} - (\Lambda_{\sigma^0})^{-1}\right] I_e\right\|_{L^2(\partial\Omega)}^2, \tag{7.15}$$

for every complete orthonormal set $\{I_e\} \subset L^2(\partial\Omega)$, the optimal approximation of (7.15), by a finite set of N functions in $L^2(\partial\Omega)$, is achieved by taking I_e as the N leading eigenvectors of self-adjoint operator $(\Lambda_\sigma)^{-1} - (\Lambda_{\sigma^0})^{-1}$. In practice, a discrete version of $(\Lambda_\sigma)^{-1}$ is measured and the optimal excitation currents I_e are calculated via an eigenvalue decomposition technique [39, 42, 72].

In the complex case ($\omega \neq 0$), where $(\Lambda_\gamma)^{-1}$ is complex symmetric, but not self-adjoint, the calculation of the optimal currents is similar to the above, the only difference being that I_e

are the right singular vectors of $(\Lambda_\sigma)^{-1} - (\Lambda_{\sigma^0})^{-1}$, instead of its eigenvectors. Finally, note that, aside from very special situations, boundary currents I_e which are optimal for the $L^2(\partial\Omega)$ norm in (7.15) do not maximize the stronger norm $\|[(\Lambda_\sigma)^{-1} - (\Lambda_{\sigma^0})^{-1}]I_e\|_{H^{\frac{1}{2}}(\partial\Omega)}$ as well (see for example [38]).

7.2.2. Variational methods. A variational, equation-error algorithm for the static ($\gamma \equiv \sigma$) EIT problem, in a slightly different form than that proposed originally by Wexler *et al* [151], has been analysed by Kohn and Vogelius [108] and implemented by Kohn and McKenney [104]. This algorithm reconstructs σ by minimizing

$$\mathcal{R}(\sigma; \phi_1, \ldots, \phi_N; \boldsymbol{j}_1, \ldots, \boldsymbol{j}_N) = \sum_{e=1}^{N} \int_\Omega \left|\sigma^{\frac{1}{2}}(\boldsymbol{x})\nabla\phi_e(\boldsymbol{x}) + \sigma^{-\frac{1}{2}}(\boldsymbol{x})\boldsymbol{j}_e\right|^2 \mathrm{d}\boldsymbol{x}, \tag{7.16}$$

over all its arguments, subject to the constraints that σ is a strictly positive function and, for all $1 \leqslant e \leqslant N$, $\phi_e(\boldsymbol{x}) = V_e(\boldsymbol{x})$, $\boldsymbol{j}_e(\boldsymbol{x}) \cdot \boldsymbol{n}(\boldsymbol{x}) = I_e(\boldsymbol{x})$ at $\partial\Omega$ and $\nabla \cdot \boldsymbol{j}_e(\boldsymbol{x}) = 0$ in Ω. This is solved with an alternate direction implicit (ADI) method in [151] and with a Newton method in [104]. Some comparisons with other reconstructions methods are given in [153].

To understand why the minimization of (7.17) is called a *variational* reconstruction method, let us expand the square in (7.16) and integrate by parts to obtain

$$\int_\Omega \left|\sigma^{\frac{1}{2}}(\boldsymbol{x})\nabla\phi_e(\boldsymbol{x}) + \sigma^{-\frac{1}{2}}(\boldsymbol{x})\boldsymbol{j}_e\right|^2 \mathrm{d}\boldsymbol{x} = \int_\Omega \sigma(\boldsymbol{x})|\nabla\phi_e(\boldsymbol{x})|^2 \,\mathrm{d}\boldsymbol{x} + \int_\Omega \sigma^{-1}(\boldsymbol{x})|\boldsymbol{j}_e(\boldsymbol{x})|^2 \,\mathrm{d}\boldsymbol{x} + 2\int_{\partial\Omega} I_e(\boldsymbol{x})V_e(\boldsymbol{x}) \,\mathrm{d}s(\boldsymbol{x}), \tag{7.17}$$

where $\int_{\partial\Omega} I_e V_e \,\mathrm{d}s$ is the measured power dissipated into heat. Then, if σ is fixed, the first two terms in (7.17) decouple; minimizing over ϕ_e is Dirichlet's variational principle (3.3) and minimizing over $\boldsymbol{j}_e$ is Thompson's variational principle (3.7).

To explain the name *equation-error*, note that the minimum of $\mathcal{R}$ is achieved when ϕ_e, the solution of Dirichlet boundary value problem (2.6), (2.7) with data V_e, is related to $\boldsymbol{j}_e$, the solution of Neumann problem (2.10), by Ohm's law (2.4). In particular, note that, since $\boldsymbol{j}_e = -\sigma(\boldsymbol{x})\nabla\psi_e(\boldsymbol{x})$, where ψ_e is the solution of Neumann boundary value problem (2.6), (2.8), (2.9) for data I_e, at the minimum, $\|\phi_e - \psi_e\|_{H^{\frac{1}{2}}(\partial\Omega)} = \|V_e - (\Lambda_\sigma)^{-1}I_e\|_{H^{\frac{1}{2}}(\partial\Omega)} = 0$, so the data are fit in the natural norm.

As expected, the ill-posedness of the EIT problem manifests itself through the lack of lower semicontinuity of the functional in (7.16), which means that, unless some regularization is added to (7.16), the iterative reconstructions of σ develop more and more oscillations and there is no convergence. Instead of choosing a standard regularization approach, Kohn and Vogelius [108] calculate the *relaxation* of variational problem (7.16), where the anticipated oscillations in σ are built directly into the functional, as is done in the homogenization of composite materials. The result is a new, lower semicontinuous problem, where σ belongs to a larger, relaxed set, containing the original admissible set of conductivities. Unfortunately, it turns out that the relaxed problem requires anisotropic, tensor-valued conductivities which cannot be determined uniquely, as explained in section 4.4. Consequently, there exists no imaging algorithm which uses Kohn and Vogelius' relaxed variational formulation of EIT, aside from a reported unsuccessful attempt in [104], so far.

7.2.3. Variational feasibility constraints Variational principles can be used in numerical reconstructions of σ, as *feasibility constraints*, as well. This idea is due to Berryman and Kohn [18] (see also [17]) and it has been implemented by Borcea, Gray and Zhang in [26, 74].

There is a variety of variational formulations based on the feasibility constraints, as explained in [26, 74], but, for brevity, we discuss just one of them, which is a modification of the output least-squares method of section 7.2.1.

Definition 3. *We say that function σ is Dirichlet feasible for boundary voltage $V_e \in H^{\frac{1}{2}}(\partial\Omega)$, if*

$$\langle V_e, \Lambda_\sigma V_e\rangle = \min_{u|_{\partial\Omega}=V_e} \int_\Omega \sigma(\boldsymbol{x})|\nabla u(\boldsymbol{x})|^2 \,\mathrm{d}\boldsymbol{x} = \int_\Omega \sigma(\boldsymbol{x})|\nabla \phi_e(\boldsymbol{x})|^2 \,\mathrm{d}\boldsymbol{x} \geqslant \langle V_e, \Lambda_{\tilde\sigma} V_e\rangle, \tag{7.18}$$

where $\tilde\sigma$ is the true conductivity and $\langle V_e, \Lambda_{\tilde\sigma} V_e\rangle = \int_{\partial\Omega} V_e I_e \,\mathrm{d}s = P_e$ is the measured power dissipated into heat. Moreover, we say that σ is Dirichlet feasible if (7.18) holds for all $V_e \in H^{\frac{1}{2}}(\partial\Omega)$.

The rationale behind this definition is given by variational principle (3.3), as follows: take any $\phi \in H^1(\Omega)$, such that $\phi|_{\partial\Omega} = V_e$ and obtain by (3.3),

$$\langle V_e, \Lambda_{\tilde\sigma} V_e\rangle \leqslant \int_\Omega \tilde\sigma(\boldsymbol{x})|\nabla\phi(\boldsymbol{x})|^2 \,\mathrm{d}\boldsymbol{x}. \tag{7.19}$$

Now, let $\phi = \phi_e$, the solution of Dirichlet problem (2.6), (2.7) for conductivity σ, and suppose that σ does not satisfy (7.18). It is clear from (7.19) that such a σ cannot be a solution and it is deemed infeasible. Similar to definition 3, we define the Thompson feasibility constraints as follows.

Definition 4. *A function σ is Thompson feasible for boundary electric current $I_e \in H^{-\frac{1}{2}}(\partial\Omega)$, if*

$$\langle I_e, (\Lambda_\sigma)^{-1} I_e\rangle = \min_{\substack{\nabla\cdot\boldsymbol{j}=0 \\ -\boldsymbol{j}\cdot\boldsymbol{n}|_{\partial\Omega}=I_e}} \int_\Omega \frac{|\boldsymbol{j}(\boldsymbol{x})|^2}{\sigma(\boldsymbol{x})} \,\mathrm{d}\boldsymbol{x} = \int_\Omega \sigma(\boldsymbol{x})|\nabla\psi_e(\boldsymbol{x})|^2 \,\mathrm{d}\boldsymbol{x} \geqslant \langle I_e, (\Lambda_{\tilde\sigma})^{-1} I_e\rangle, \tag{7.20}$$

where $\boldsymbol{j}_e = -\sigma\nabla\psi_e$ and $\langle I_e, (\Lambda_{\tilde\sigma})^{-1} I_e\rangle = \int_{\partial\Omega} V_e I_e \,\mathrm{d}s = P_e$, the measured power dissipated into heat. Moreover, σ is Thompson feasible, if (7.20) holds for all $I_e \in H^{-\frac{1}{2}}(\partial\Omega)$.

Finally, we say that σ is feasible if it is both Dirichlet and Thompson feasible.

For simplicity, let us drop the indices e from the notation and say that V and I are our generic boundary data and $P = \int_{\partial\Omega} IV \,\mathrm{d}s$. Suppose that we have an iterative reconstruction process which generates a sequence $\{\sigma^{(k)}\}_{k\geqslant 1}$ of conductivities such that

$$\lim_{k\to\infty} \langle I, (\Lambda_{\sigma^{(k)}})^{-1} I\rangle \to P \qquad \text{and} \qquad \lim_{k\to\infty} \langle V, \Lambda_{\sigma^{(k)}} V\rangle \to P. \tag{7.21}$$

Since for any σ, $\langle I, (\Lambda_\sigma)^{-1} I\rangle + \langle V, \Lambda_\sigma V\rangle - 2P = \int_\Omega \sigma(\boldsymbol{x})|\nabla\phi(\boldsymbol{x}) - \nabla\psi(\boldsymbol{x})|^2 \,\mathrm{d}\boldsymbol{x}$, (7.21) implies

$$\lim_{k\to\infty} \int_\Omega \sigma(\boldsymbol{x})|\nabla\phi^{(k)}(\boldsymbol{x}) - \nabla\psi^{(k)}(\boldsymbol{x})|^2 \,\mathrm{d}\boldsymbol{x} = 0, \tag{7.22}$$

where $\phi^{(k)}$ and $\psi^{(k)}$ are the Dirichlet and Thompson potentials for conductivity $\sigma^{(k)}$. Then, by the coercivity of bilinear form $a(u, w) = \int_\Omega \sigma^{(k)} \nabla u \cdot \nabla w \,\mathrm{d}\boldsymbol{x}$, for $u, w \in H^1(\Omega)$ satisfying $\int_{\partial\Omega} u \,\mathrm{d}s = \int_{\partial\Omega} w \,\mathrm{d}s = 0$ (see [68]), $\lim_{k\to\infty} \|\phi^{(k)} - \psi^{(k)}\|_{H^1(\Omega)} = 0$ and, by the trace theorem [68], $\lim_{k\to\infty} \|V - (\Lambda_{\sigma^{(k)}})^{-1} I\|_{H^{\frac{1}{2}}(\partial\Omega)} = 0$. Therefore, any sequence $\{\sigma^{(k)}\}_{k\geqslant 1}$ which gives (7.21), fits the measurements in the $H^{\frac{1}{2}}(\partial\Omega)$ norm.

Now, suppose that we have an output least-squares method, which generates a sequence $\{\sigma^{(k)}\}_{k\geqslant 1}$ such that

$$\lim_{k\to\infty} \|V - \Lambda_{\sigma^{(k)}} I\|_{L^2(\partial\Omega)} = 0. \tag{7.23}$$

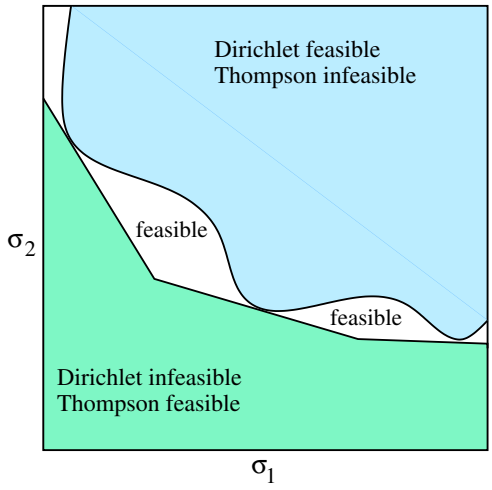

Figure 4. The Thompson infeasibility region is contained in the Dirichlet feasible region. The convergence result (7.24) does not imply the convergence of the Dirichlet constraint to P, unless σ is restricted to the Dirichlet infeasible region.

Since $\langle I, (\Lambda_\sigma)^{-1} I\rangle - P = \int_{\partial\Omega} I[(\Lambda_\sigma)^{-1} I - V]\,\mathrm{d}s$, for any σ, we can achieve convergence of the Thompson constraint

$$\lim_{k\to\infty} \langle I, (\Lambda_{\sigma^{(k)}})^{-1} I\rangle = P, \tag{7.24}$$

by choosing an excitation $I \in L^2(\partial\Omega)$. However, for the Dirichlet constraint, we have (see [26, 74])

$$\langle V, \Lambda_{\sigma^{(k)}} V\rangle - P = \int_{\partial\Omega} [V(\boldsymbol{x}) - (\Lambda_{\sigma^{(k)}})^{-1} I(\boldsymbol{x})]\Lambda_{\sigma^{(k)}} V(\boldsymbol{x})\,\mathrm{d}s(\boldsymbol{x}), \tag{7.25}$$

and convergence does not follow since $\Lambda_{\sigma^{(k)}} V \in H^{-\frac{1}{2}}(\partial\Omega)$ is not in general also in $L^2(\partial\Omega)$.

In [26, 74] it is shown that convergence of (7.25) can be achieved by an output least-squares method, if we make use of the feasibility constraints. This is because, as is proved in [26, 74], the Thompson infeasibility region for any $I \in H^{-\frac{1}{2}}(\partial\Omega)$ is contained within the Dirichlet feasibility region for the measured $V = (\Lambda_{\tilde\sigma})^{-1} I \in H^{\frac{1}{2}}(\partial\Omega)$. Hence, convergence of (7.25) follows from (7.23) if $I \in L^2(\partial\Omega)$ and we restrict all iterates to the Dirichlet infeasibility region, as illustrated in figure 4 for a conductivity function that can take two values, σ_1 and σ_2. This is the basic idea of the variational method proposed in [26, 74], where the authors minimize objective function (7.13), subject to constraints

$$\langle V_e, \Lambda_\sigma V_e\rangle \leqslant \langle V_e, \Lambda_{\tilde\sigma} V_e\rangle, \qquad \text{for all } e = 1, \ldots, N. \tag{7.26}$$

The constrained nonlinear optimization problem is solved in [26, 74] with an interior point method [119]. The algorithm is tested numerically and it is compared with other, standard imaging methods. In particular, it is shown that in many cases, the constrained variational method performs better than output least squares. Although both methods require regularization, it is found in [26, 74] that, for the same regularization parameters, output least squares give a poorer quality of the images. Finally, the variational constraints can be incorporated in the reconstruction algorithm at a very small computational cost (see [26, 74]), so they may be a worthwhile addition to standard output least-squares methods.

7.2.4. Regularity of the forward map Consider definition (7.11) of the forward map. To *linearize* the problem in the vicinity of admittivity $\gamma \in \Upsilon$, we consider a small perturbation $\delta\gamma$, such that $\gamma + \delta\gamma \in \Upsilon$ and we approximate the perturbation of the electric potential by $\delta\phi$, where

$$\begin{aligned} &\nabla \cdot [\gamma(\boldsymbol{x}, \omega)\nabla\delta\phi(\boldsymbol{x}, \omega)] = -\nabla \cdot [\delta\gamma(\boldsymbol{x}, \omega)\nabla\phi(\boldsymbol{x}, \omega)] \qquad \text{in } \Omega, \\ &\frac{\partial\delta\phi(\boldsymbol{x}, \omega)}{\partial n} = 0 \qquad \text{at } \partial\Omega, \\ &\int_{\partial\Omega} \delta\phi(\boldsymbol{x}, \omega)\, \mathrm{d}s(\boldsymbol{x}) = 0, \end{aligned} \tag{7.27}$$

and where ϕ is the solution of (2.6), (2.8), (2.9), for admittivity γ. We have the following result.

Theorem 5. *For an arbitrary $I \in \mathcal{J}$, the forward map $F[\gamma, I]$ defined by (7.10), (7.11), is continuous and Fréchet differentiable with respect to γ. The Fréchet derivative is denoted by $DF[\gamma, I]$ and it is given by*

$$(DF[\gamma, I]\delta\gamma)(\boldsymbol{x}, \omega) = \delta\phi(\boldsymbol{x}, \omega), \qquad \textit{for } \boldsymbol{x} \in \partial\Omega. \tag{7.28}$$

See [53] for a proof of regularity estimates

$$\|F[\gamma + \delta\gamma, I] - F[\gamma, I]\|_{L^2(\partial\Omega)} \leqslant C_1 \|\delta\gamma\|_{L^\infty(\partial\Omega)}, \tag{7.29}$$

$$\|F[\gamma + \delta\gamma, I] - F[\gamma, I] - DF[\gamma, I]\delta\gamma\|_{L^2(\partial\Omega)} \leqslant C_2 \|\delta\gamma\|^2_{L^\infty(\partial\Omega)}, \tag{7.30}$$

where C_1 and C_2 are some bounded constants.

In numerical computations, it is not convenient to work with the solution space $L^\infty(\overline{\Omega})$. It is preferable to work with a Hilbert solution space, for example $L^2(\Omega)$, such that we can use integration by parts and calculate easily the derivatives of the objective function (see section 7.2.5). Unfortunately, estimates such as (7.29) and (7.30), but with the $L^2(\Omega)$ norm of $\delta\gamma$ in the right-hand side, are not necessarily true for $\gamma \in \Upsilon$. It turns out that, in order to get the desired $L^2(\Omega)$ regularity estimates, the electric potential ϕ must belong to $W^{1,\infty}(\Omega)$ (see [53]). A sufficient condition for such a result to hold is that $\gamma \in C^{k,1}(\Omega) \cap \Upsilon$, for $k > n/2 - 1$ [53]. However, it is easy to see that there exist many functions $\gamma(\boldsymbol{x}, \omega)$ which are not even continuous, and they still give $\phi \in W^{1,\infty}(\Omega)$ (see [20, 112] for two such examples). In fact, it is not known what is the necessary degree of smoothness that γ has to satisfy in order to get the desired $L^2(\Omega)$ regularity of forward map F.

Some numerical reconstruction algorithms require the second derivative of the forward map. For $\gamma \in \Upsilon$, the bilinear second derivative operator $D^2F[\gamma, I](\cdot, \cdot)$ can be defined on the solution space $L^\infty(\Omega)$, or on $L^2(\Omega)$, with additional assumptions on γ (see [53]). Explicitly, we have

$$D^2F[\gamma, I](\delta\gamma, \delta\gamma) = \delta^2\phi(\boldsymbol{x}, \omega), \qquad \text{for } \boldsymbol{x} \in \partial\Omega, \tag{7.31}$$

where $\delta^2\phi$ solves

$$\begin{aligned} &\nabla \cdot [\gamma(\boldsymbol{x}, \omega)\nabla\delta^2\phi(\boldsymbol{x}, \omega)] = -\nabla \cdot [\delta\gamma(\boldsymbol{x}, \omega)\nabla\delta\phi(\boldsymbol{x}, \omega)] \qquad \text{in } \Omega, \\ &\frac{\partial\delta^2\phi(\boldsymbol{x}, \omega)}{\partial n} = 0 \qquad \text{at } \partial\Omega, \\ &\int_{\partial\Omega} \delta^2\phi(\boldsymbol{x}, \omega)\, \mathrm{d}s(\boldsymbol{x}) = 0. \end{aligned} \tag{7.32}$$

7.2.5. The adjoint derivatives of the forward map. Choose an $I = I_e$, for some $e \leqslant N$ in (7.13) and fix it, such that we can view F as a function of γ only. Assuming that F is Fréchet differentiable, as a map from $L^2(\Omega)$ to $L^2(\partial\Omega)$, the gradient of

$$\mathcal{G}[\gamma] = \tfrac{1}{2}\left\|\left((\Lambda_\gamma)^{-1} - (\Lambda_{\tilde{\gamma}})^{-1}\right)I\right\|^2_{L^2(\partial\Omega)} \tag{7.33}$$

is given by

$$D\mathcal{G}[\gamma](\boldsymbol{x}, \omega) = DF^A[\gamma]\left((\Lambda_\gamma)^{-1} - (\Lambda_{\tilde{\gamma}})^{-1}\right)I(\boldsymbol{x}, \omega) \qquad \text{for } \boldsymbol{x} \in \Omega, \tag{7.34}$$

where $DF^A[\gamma]$ is the $L^2(\partial\Omega) \to L^2(\Omega)$ adjoint of $DF[\gamma]$. The adjoint method gives a very efficient way of calculating the gradient $D\mathcal{G}[\gamma]$, as follows.

Lemma 5. *Let $\chi(\boldsymbol{x}, \omega) = [(\Lambda_\gamma)^{-1} - (\Lambda_{\tilde{\gamma}})^{-1}]I(\boldsymbol{x}, \omega)$ be defined for $\boldsymbol{x} \in \partial\Omega$ and note that by (2.9), $\int_{\partial\Omega} \chi(\boldsymbol{x}, \omega)\, \mathrm{d}s(\boldsymbol{x}) = 0$. We have*

$$DF^A[\gamma]\chi(\boldsymbol{x}, \omega) = -\nabla\phi^\star(\boldsymbol{x}, \omega) \cdot \psi(\boldsymbol{x}, \omega) \qquad \textit{for } \boldsymbol{x} \in \Omega, \tag{7.35}$$

where ϕ is the solution of (2.6), (2.8) and (2.9) and ψ solves the adjoint problem

$$\begin{aligned} &\nabla \cdot [\gamma^\star(\boldsymbol{x}, \omega)\nabla\psi(\boldsymbol{x}, \omega)] = 0 \qquad \textit{in } \Omega, \\ &\gamma^\star(\boldsymbol{x}, \omega)\frac{\partial\psi(\boldsymbol{x}, \omega)}{\partial n} = \chi(\boldsymbol{x}, \omega) \qquad \textit{at } \partial\Omega, \\ &\int_{\partial\Omega} \psi(\boldsymbol{x}, \omega)\, \mathrm{d}s(\boldsymbol{x}) = 0. \end{aligned} \tag{7.36}$$

Proof. Take an arbitrary perturbation $\delta\gamma$, such that $\gamma + \delta\gamma \in \Upsilon$. In particular, this implies that $\delta\gamma$ vanishes at $\partial\Omega$. Integration by parts, (7.27) and (7.36) give

$$\begin{aligned} \langle DF\delta\gamma, \chi\rangle &= \int_{\partial\Omega} \delta\phi^\star\gamma^\star\frac{\partial\psi}{\partial n}\, \mathrm{d}s = \int_{\partial\Omega}\left(\delta\phi^\star\gamma^\star\frac{\partial\psi}{\partial n} - \psi\gamma^\star\frac{\partial\delta\phi^\star}{\partial n}\right)\mathrm{d}s \\ &= \int_\Omega \nabla\cdot(\delta\phi^\star\gamma^\star\nabla\psi - \psi\gamma^\star\nabla\delta\phi^\star)\, \mathrm{d}\boldsymbol{x} = -\int_\Omega \psi\nabla\cdot(\gamma^\star\nabla\delta\phi^\star)\, \mathrm{d}\boldsymbol{x} \\ &= \int_\Omega \psi\nabla\cdot(\delta\gamma^\star\nabla\phi^\star)\, \mathrm{d}\boldsymbol{x} = -\int_\Omega \delta\gamma^\star\nabla\psi\cdot\nabla\phi^\star\, \mathrm{d}\boldsymbol{x} = (\delta\gamma, DF^A\chi), \end{aligned}$$

where $(\cdot, \cdot)$ is the $L^2(\Omega)$ inner product. □

The most efficient numerical optimization methods (for example, Newton's method), require inverting the Hessian of the objective function [49]. While the calculation of the Hessian can be very expensive, the adjoint method allows us to calculate the Hessian times a vector and it can be used for inverting the Hessian in an iterative manner. To get the second derivative of $\mathcal{G}$, in direction $\delta\gamma$, we do another integration by parts, similar to the above, and we obtain

$$D^2\mathcal{G}\delta\gamma(\boldsymbol{x}, \omega) = DF^A[\gamma]DF[\gamma]\delta\gamma(\boldsymbol{x}, \omega) + (D^2F[\gamma])^A(\chi, \delta\gamma)(\boldsymbol{x}, \omega) \qquad \text{for } \boldsymbol{x} \in \Omega, \tag{7.37}$$

where $(D^2F[\gamma])^A(\cdot, \cdot)$ is a bilinear form on $L^2(\partial\Omega) \times L^2(\Omega)$, given explicitly by

$$(D^2F[\gamma])^A(\chi, \delta\gamma)(\boldsymbol{x}, \omega) = -\nabla\delta\phi^\star(\boldsymbol{x}, \omega)\cdot\nabla\psi(\boldsymbol{x}, \omega). \tag{7.38}$$

We conclude this section with the final note that both (7.35) and (7.38) imply inverting the same differential operator that appears in the forward problem (see (2.6), (2.8) and (2.9)). Therefore, once the forward problem is solved, the gradient of $\mathcal{G}$ and its Hessian times a vector are given by the adjoint method, at a very low computational cost.

7.3. Multigrid

Typically, iterative nonlinear optimization algorithms for EIT (see section 7.2) can be very costly, especially in three dimensions. A natural idea for reducing the computational cost is to use multigrid (multilevel) methods, as shown in [8, 22, 98, 102, 113] and the references within. In a multigrid setting, the unknown γ (and perhaps the electric potential) is projected on a sequence of nested, finite-dimensional spaces $\mathcal{Y}_0 \subset \mathcal{Y}_1 \subset \mathcal{Y}_2 \subset \cdots$ whose union is dense in the solution space. For instance, if we seek $\gamma \in H^1(\overline{\Omega})$, Ω is discretized on a sequence of nested grids $G_0, G_1, G_2 \ldots$ and $\mathcal{Y}_j$ can be taken as the set of piecewise linear functions on G_j, for $j \geqslant 0$.

Take, for example, the output least-squares problem (7.13), with regularization $\alpha\|\nabla\gamma\|^2_{L^2(\Omega)}$, such that a minimizer γ satisfies the semilinear elliptic equation

$$-\alpha\Delta\gamma(\boldsymbol{x},\omega) + \sum_{e=1}^{N} DF^A[\gamma]\big[(\Lambda_\gamma)^{-1}I_e - V_e\big](\boldsymbol{x},\omega) = 0. \tag{7.39}$$

Multigrid algorithms can be very efficient solvers of equations like (7.39) because they perform a large part of the work on the coarser grids, where computations are cheap and the problem is less ill-posed [8, 22, 98, 102, 113]. Typically, the best performance is expected when the first term in (7.39) dominates (α large enough), although, to get a reasonable resolution of γ, a small α is needed. Therefore, it is important to have a good initial guess of γ, such that the first term in (7.39) dominates the nonlinear and ill-conditioned one, even for small α. Such a guess can be calculated on the coarsest grid G_0, where, due to the coarse discretization, the problem is less ill-posed. This idea is pursued in [22, 98], in a nested iteration (full multigrid) which constructs the images of γ sequentially, starting from the coarse grid G_0 and moving towards the finest one G_m.

In order to succeed, the coarse-grid computations require an accurate solution of the forward problem, which means, for example, solving equations (2.6), (2.8) on a fine grid (like G_m). Another approach is given in [22], where the excitation current I_e is restricted to the boundary $\delta G_0 = G_0 \cap \partial\Omega$ in such a way that the potential at ∂G_0 is accurate, in spite of the coarse discretization of equations (2.6), (2.8). Explicitly, let $\gamma^{(0)}$ be a coarse-grid admittivity, which is the restriction, or at least an approximation of $\tilde{\gamma}$, on G_0. The coarse-grid current $I_e^{(0)}(\gamma^{(0)})$ is defined by

$$R_{0\leftarrow m}(\Lambda_{\gamma^{(m)}})^{-1}I_e = (\Lambda_{\gamma^{(0)}})^{-1}I_e^{(0)}(\gamma^{(0)}), \qquad \gamma^{(m)} = P_{m\leftarrow 0}\gamma^{(0)}, \tag{7.40}$$

where $R_{0\leftarrow m}$ and $P_{m\leftarrow 0}$ are restriction and interpolation operators between grids G_0 and G_m, and $(\Lambda_{\gamma^{(m)}})^{-1}$, $(\Lambda_{\gamma^{(0)}})^{-1}$ are the discrete approximations of the NtD map on G_0 and G_m, respectively. Assuming that both $\gamma^{(m)}$ and $\gamma^{(0)}$ are reasonable approximations of the true $\tilde{\gamma}$, definition (7.40) ensures that, on G_0, the boundary voltage is a good approximation of the measured V_e. Although $I_e^{(0)}$ is a nonlinear function of the unknown $\gamma^{(0)}$, it turns out that the dependence is weak and, for a perturbation $\delta\gamma^{(0)}$ of $\gamma^{(0)}$, $\delta(\Lambda_{\gamma^{(0)}})I_e^{(0)}(\gamma^{(0)}) \gg (\Lambda_{\gamma^{(0)}})\delta I_e^{(0)}(\gamma^{(0)})$, as shown in [22]. Then, based on this sensitivity result, $\gamma^{(0)}$ and $I_e^{(0)}$ are calculated iteratively in [22], with just a few fine-grid solutions needed to update $I_e^{(0)}$ (see (7.40)).

Although the behaviour of nonlinear multigrid methods is not so well understood, for linearized EIT, there exists a very nice proof of the regularization properties of full multigrid (nested iteration), due to Kaltenbacher [98]. Finally, Ascher and Haber [8] take a different approach to multilevel reconstruction, which is based on the ansatz that the solution of (7.39) (or another, similar formulation) depends continuously on the regularization parameter and they estimate α on the coarse grid.

7.4. Optimal finite-difference grids

In any numerical reconstruction algorithm, the unknown σ (or γ) must be parametrized or discretized. There are many possible parametrizations of γ, in a Fourier basis [7, 33], a wavelet basis [54], a set of high-contrast functions [23, 24], etc. We consider here a more general parametrization, where γ is restricted on a grid G which discretizes Ω. In most numerical algorithms, G is an equidistant grid, although this is not a good choice, as suggested by studies of distinguishability of σ (see section 6.2 and [7, 38, 42, 52, 54]). Since it is easier to detect inhomogeneities of σ near $\partial\Omega$, a better discretization would be on an adaptive grid G, with steps growing progressively from $\partial\Omega$, inside the domain.

Although in general it is not known how to define optimal grids, a solution has been obtained by Borcea and Druskin in [25] for layered media occupying a strip space in $\mathbb{R}^d$, for $d \geqslant 2$. Let $\sigma(z)$ be the conductivity in a strip $\Omega = \{(x_1, \ldots, x_{d-1}, z) \in \mathbb{R}^d, 0 \leqslant z \leqslant L \leqslant \infty\}$, where the bottom boundary $z = L$ is grounded and the excitation current $I(x_1, \ldots, x_{d-1})$ is confined to the surface $z = 0$. The electric potential ϕ satisfies

$$\begin{aligned} &\nabla \cdot [\sigma(z)\nabla\phi(x, y, z)] = 0 \qquad \text{in } \Omega, \\ &-\sigma(0)\frac{\partial\phi}{\partial z}(x, y, 0) = I(x, y), \qquad \phi(x, y, L) = 0. \end{aligned}$$

Let us take the Fourier transform with respect to $x_1, \ldots, x_{d-1}$ and obtain

$$\begin{aligned} &\frac{\mathrm{d}}{\mathrm{d}z}\left[\sigma(z)\frac{\mathrm{d}u(z;\lambda)}{\mathrm{d}z}\right] - \lambda\sigma(z)u(z;\lambda) = 0, \qquad \text{for } 0 < z < L, \\ &-\sigma(0)\frac{\mathrm{d}u(0;\lambda)}{\mathrm{d}z} = 1, \qquad u(L;\lambda) = 0, \end{aligned} \tag{7.41}$$

where

$$u(z) = \frac{\hat{\phi}(k_1, \ldots, k_{d-1}, z)}{\hat{I}(k_1, \ldots, k_{d-1})} \qquad \text{and} \qquad \lambda = \sum_{i=1}^{d-1} k_i^2.$$

Further, introduce the coordinate transformation $y(z) = \int_0^z 1/\sigma(s)\,\mathrm{d}s$ and define the monotonically increasing, continuous function $M : [0, l] \to [0, \hat{l}]$, $M(y(z)) = \hat{y}(z) = \int_0^z \sigma(s)\,\mathrm{d}s$, where $l = x(L)$ and $\hat{l} = \hat{x}(L)$, such that (7.41) becomes

$$\begin{aligned} &\frac{\mathrm{d}}{\mathrm{d}M(y)}\left[\frac{\mathrm{d}u(y;\lambda)}{\mathrm{d}y}\right] - \lambda u(y;\lambda) = 0, \qquad \text{for } 0 < y < l \leqslant \infty, \\ &-\frac{\mathrm{d}u(0;\lambda)}{\mathrm{d}y} = 1, \qquad u(l;\lambda) = 0, \end{aligned} \tag{7.42}$$

the equation of motion of a string with a fixed right endpoint, oscillating at frequency $\sqrt{\lambda}$, under a Neumann excitation at the left endpoint. At coordinate y along the string, the mass distribution is given by $M(y)$, the primitive of σ, which we wish to find, given measurements of impedance $f(\sigma;\lambda_i) = u(0;\lambda_i)$, for $2m$ noncoinciding spectral parameters λ_i. Impedance functions $f(\sigma;\lambda)$ of such strings are completely characterized in [95]. In particular, it is shown there that $f(\sigma;\lambda)$ is a Stieljes function, written in terms of its spectral measure μ, as

$$f(\sigma;\lambda) = \int_{-\infty}^{0} \frac{\mathrm{d}\mu(s)}{\lambda - s}. \tag{7.43}$$

If the length l of the string is finite, measure μ is discrete and $f(\sigma;\lambda)$ has an infinite number of distinct, negative poles ξ_n and positive residues r_n, for $n \geqslant 1$. If l is infinite, the spectrum of measure μ is continuous.

A finite-difference discretization of (7.42) is

$$\frac{1}{\hat{\eta}_j}\left(\frac{U_{j+1}-U_j}{\eta_j}-\frac{U_j-U_{j-1}}{\eta_{j-1}}\right)-\lambda U_j=0, \qquad \text{for } j=1,2\ldots m,$$

$$-\frac{U_1-U_0}{\eta_0}=1, \qquad U_{m+1}=0,$$

where

$$\eta_i=\int_{z_i}^{z_{i+1}}\frac{\mathrm{d}s}{\sigma(s)}, \qquad \hat{\eta}_i=\int_{\hat{z}_{i-1}}^{\hat{z}_i}\sigma(s)\,\mathrm{d}s, \qquad \text{for } 1\leqslant i\leqslant m \tag{7.44}$$

and the string is partitioned by primary nodes $\{z_i\}_{i=1}^{m+1}$, and dual nodes $\{\hat{z}_i\}_{i=0}^{m}$, such that $z_1=\hat{z}_0=0$. Similar to (7.42), discrete equations (7.44) describe the motion of a Stieljes string of m discrete masses $\hat{\eta}_j$ placed at coordinates $y_j=\sum_{i=1}^{j-1}\eta_i$, $y_1=0$, and a piecewise constant, monotone increasing mass distribution $M_m(y)=\sum_{y_j\leqslant y}\hat{\eta}_j$, for any $y\in[0,l]$. Finally, the discrete impedance is a rational function

$$f_m(\sigma;\lambda)=\sum_{p=1}^{m}\frac{\zeta_p}{\lambda-\theta_p}, \tag{7.45}$$

with negative poles θ_p and positive residues ζ_p, given by the eigenvalues and squares of the first components of the eigenvectors of the discrete difference operator in (7.44), respectively (see [60, 61, 87]).

The optimal finite-difference grids are defined such that the discrete impedance $f_m(\sigma;\lambda)$ converges to $f(\sigma;\lambda)$, at an *exponential* rate, as $m\to\infty$. These grids are introduced and analysed by Druskin and Knizhnerman in [60, 61] and, in collaboration with Ingerman and Moskow, in [87] and [62], respectively. They are used for the first time in imaging by Borcea and Druskin in [25]. It is clear that $f_m(\sigma;\lambda)$ is completely determined by the coefficients (7.44) and these can be found uniquely, by letting f_m be the multipoint Padé approximant of Stieljes function (7.43) and solving a discrete inverse eigenvalue problem [43], respectively. The details of this calculation are given in [60, 61, 87]. Then, if we knew σ, the grid would be obtained immediately from (7.44). This is done in the numerical solution of forward problems and some properties of the optimal grids are proved in [25, 87]. However, in inversion, σ is not known and, in order to find it, we must define the grid. Of course, we cannot choose an arbitrary grid, because, as shown in [25], the discrete solution diverges due to false anisotropy, i.e. noncoinciding curves of σ at the primary and dual points, respectively. It is proved in [25] and confirmed by extensive numerical experiments that the grid has to be close to the optimal one, in order to get convergence. Fortunately, as shown in [25], the optimal grids depend weakly on σ, although strongly on the spectral interval. Consequently, the reconstructions can be done on the optimal grid calculated for a known σ, say a constant, and convergence to the solution is obtained in the limit $m\to\infty$. The analysis in [25] suggests that this should work for smooth σ but the numerical experiments show convergence even for conductivities with jump discontinuity.

Clearly, there is much work to be done on optimal grids, even for the forward problem, for more general conductivities σ, domains Ω and boundary conditions. Nevertheless, the setup presented here has proved very useful for both forward and inverse problems in geophysics and extensions to forward problems for Maxwell's equations [132] and hyperbolic equations [9] have been made, as well.

8. Other electromagnetic inverse problems related to EIT

Magnetotellurics [150, 152] is another low-frequency, electromagnetic method for imaging the conductivity σ of heterogeneous media. Unlike EIT, magnetotellurics arises strictly in geophysics applications and it uses naturally occurring, ambient electromagnetic radiation, instead of the NtD map, which requires man-forced excitation. Nevertheless, EIT and magnetotellurics have many similarities, like the limited accuracy and spatial resolution, due to the diffusive behaviour of low-frequency electromagnetic propagation in the medium.

For higher-frequency electromagnetic fields in conductive materials, the EIT model is not appropriate and the full system of Maxwell's equations must be considered. This problem is much more difficult than EIT, and there are few theoretical results (see for example [93]). The numerical solution of the inverse problem is also less studied, especially in three dimensions where computations are very expensive, but there is nice progress in works such as [55, 56, 77, 78, 137] and the references within.

Finally, we mention the interesting work done by Cherkaeva [41] on inverse homogenization, where the admittivity of a random mixture of two materials is to be determined from measurements of the effective (homogenized) admittivity, at various frequencies. Cherkaeva's approach is based on the Stieljes integral representation of the effective admittivity [15, 73, 114], where the geometric information about the mixture is entirely contained in the measure μ. In general, the mixture cannot be determined uniquely, because there exist quite different geometries that give the same effective admittivity. However, the spectral measure μ is uniquely identifiable by measurements of the effective admittivity over a spectral interval and its moments can be used to extract useful information, such as the volume fraction of the components in the mixture.

9. Conclusions

We have discussed EIT, the inverse problem of determining the electrical conductivity and permittivity inside a domain, given simultaneous measurements of electric currents and potentials (the NtD or DtN map) at the boundary. Although this problem has been extensively studied in the last two decades, it remains an area of active research, with many open questions to be addressed. Examples of open problems are:

- Most of the theoretical results on the injectivity of the inverse map assume perfect knowledge of the DtN map at the boundary. In practice, this is not the case and, furthermore, the model has to be changed to account for the electrodes. In such a setup, injectivity remains to be investigated.
- It is not clear in most cases how to discretize (parametrize) the unknown conductivity or admittivity. For example, a wavelet parametrization seems very promising but it needs to be fully investigated. Optimal grids have been proposed recently for layered media. Extensions to more general problems remain to be made. Studies of distinguishability have been made only for the static ($\omega = 0$) case. In the complex admittivity problem, distinguishability is not understood.
- Imaging of anisotropic media is very little understood. Even though uniqueness of solutions does not hold, it may be that some useful information can be extracted from the data.
- Imaging of high-contrast media of the type presented in section 5 requires more study.
- Variational reconstruction methods for the complex admittivity problem have not been studied, so far.

- There remain many questions on how to properly regularize the EIT problem. Multigrid is a promising alternative but it is not completely understood, especially for nonlinear EIT.
- In many applications, the conductivity function consists of a smooth part and a highly oscillatory, random part. The question is how to model the effect of the random fluctuations on the measured boundary data and ultimately extract the smooth part of σ. Such a problem has been studied in [152] for magnetotellurics, in layered media, but not for EIT and more general materials.

Acknowledgments

This review is based on the author's lectures at the Mathematical Sciences Research Institute's workshop on Inverse Problems, August, 2001. I am very grateful to Professors Grünbaum and Uhlmann for their kind invitation and the opportunity to participate in such a nice programme. Most of the material has been prepared while visiting the department of mathematics at Stanford University. I am very grateful to my host, Professor Papanicolaou, for his support and input on this paper.

This work was partially supported by the National Science Foundation under grant number DMS-9971209 and by the Office of Naval Research, under grant N00014-02-1-0088.

References

[1] Akbarzadeh M R, Tompkins W J and Webster J G 1990 Multichannel impedance pneumography for apnea monitoring *Proc. Ann. Int. Conf. IEEE Eng. Med. Biol. Soc.* vol 12 pp 1048–9
[2] Alessandrini G 1988 Stable determination of conductivity by boundary measurements *Appl. Anal.* **27** 153–72
[3] Alessandrini G 1993 Stable determination of a crack from boundary measurements *Proc. R. Soc. Edin.* A **127** 497–516
[4] Alessandrini G 1997 Examples of instability in inverse boundary-value problems *Inverse Problems* **13** 887–97
[5] Alessandrini G, Beretta E, Santosa F and Vessella S 1995 Stability in crack determination from electrostatic measurements at the boundary-a numerical investigation *Inverse Problems* **11** L17–24
[6] Alessandrini G and Rondi L 1998 Stable determination of a crack in a planar inhomogeneous conductor *SIAM J. Math. Anal.* **30** 326–40
[7] Allers A and Santosa F 1991 Stability and resolution analysis of a linearized problem in electrical impedance tomography *Inverse Problems* **7** 515–33
[8] Ascher U M and Haber E 2001 Grid refinement and scaling for distributed parameter estimation problems *Inverse Problems* **17** 571–90
[9] Asvadurov S, Druskin V and Knizhnerman L 2000 Application of the difference Gaussian rules to solution of hyperbolic problems *J. Comput. Phys.* **158** 116–35
[10] Barber D and Brown B 1984 Applied potential tomography *J. Phys. E: Sci. Instrum.* **17** 723–33
[11] Barber D and Brown B 1986 Recent developments in applied potential tomography-apt *Information Processing in Medical Imaging* ed S L Bacharach (Amsterdam: Nijhoff) pp 106–21
[12] Batchelor G K and O'Brien R W 1977 Thermal or electrical conduction through a granular material *Proc. R. Soc.* A **355** 313–33
[13] Bensousaan A, Lions J L and Papanicolaou G C 1978 *Asymptotic Analysis for Periodic Structures* (Amsterdam: North-Holland)
[14] Berenstein C A and Casadio Tarabusi E 1996 Integral geometry in hyperbolic spaces and electrical impedance tomography *SIAM J. Appl. Math.* **56** 755–64
[15] Bergman D J 1993 Hierarchies of Stieljes functions and their applications to the calculation of bounds for the dielectric constant of a two component composite medium *SIAM J. Appl. Math.* **53** 915–30
[16] Berlyand L and Kolpakov A 2001 Network approximation in the limit of small interparticle distance of the effective properties of a high-contrast random dispersed composite *Arch. Ration. Mech. Anal.* **159** 179–227
[17] Berryman J G 1991 Convexity properties of inverse problems with variational constraints *J. Franklin Institute* **328** 1–13
[18] Berryman J G and Kohn R V 1990 Variational constraints for electrical impedance tomography *Phys. Rev. Lett.* **65** 325–8

[19] Beylkin G 1984 The inversion problem and applications of the generalized Radon transform *Commun. Pure Appl. Math.* **37** 580–99
[20] Bonnetier E and Vogelius M 2000 An elliptic regularity results for a composite medium with 'touching' fibers of circular cross-section *SIAM J. Math. Anal.* **93** 651–77
[21] Borcea L 1999 Asymptotic analysis of quasi-static transport in high contrast conductive media *SIAM J. Appl. Math.* **59** 597–635
[22] Borcea L 2001 A nonlinear multigrid for imaging electrical conductivity and permittivity at low frequency *Inverse Problems* **17** 329–59
[23] Borcea L, Berryman J G and Papanicolaou G C 1996 High contrast impedance tomography *Inverse Problems* **12** 935–58
[24] Borcea L, Berryman J G and Papanicolaou G C 1999 Matching pursuit for imaging high contrast conductive media *Inverse Problems* **15** 811–49
[25] Borcea L and Druskin V 2002 Optimal finite difference grids for direct and inverse Sturm–Liouville problems *Inverse Problems* **18** 1247–79
[26] Borcea L, Gray G and Zhang Y 2002 A variationally constrained numerical solution of the electrical impedance tomography problem *Preprint* (*Inverse Problems* to be submitted)
[27] Borcea L and Papanicolaou G C 1998 Network approximation for transport properties of high contrast materials *SIAM J. Appl. Math.* **58** 501–39
[28] Borcea L and Papanicolaou G C 2000 Low frequency electromagnetic fields in high contrast media *Surveys on Solution Methods for Inverse Problems* ed D Colton, H W Engl, A Louis, J R McLaughlin and W Rundell (New York: Springer) pp 195–233
[29] Brown R M 1996 Global uniqueness in the impedance imaging problem for less regular conductivities *SIAM J. Math. Anal.* **27** 1049–56
[30] Brown R M and Uhlmann G 1997 Uniqueness in the inverse conductivity problem for nonsmooth conductivities in two dimensions *Commun. Part. Diff. Eqns* **22** 1009–27
[31] Brühl M and Hanke M 2000 Numerical implementation of two noniterative methods for locating inclusions by impedance tomography *Inverse Problems* **16** 1029–42
[32] Calderón A P 1963 Boundary value problems for elliptic equations *Outlines of the Joint Soviet–American Symp. on Partial Differential Equations (Novosibirsk)* pp 303–4
[33] Calderón A P 1980 On an inverse boundary value problem *Seminar on Numerical Analysis and its applications to Continuum Physics (Soc. Brasileira de Matèmatica, Rio de Janeiro)* pp 65–73
[34] Cedio-Fengya D J, Moskow S and Vogelius M S 1998 Identification of conductivity imperfections of small diameter by boundary measurements. continuous dependence and computational reconstruction *Inverse Problems* **14** 553–95
[35] Chan T, Golub G H and Mulet P 1999 A nonlinear primal-dual method for total variation-based image restoration *SIAM J. Sci. Comput.* **20** 1964–77
[36] Chavent G and Kunisch K 1993 Regularization in state space *J. Numer. Anal.* **27** 535–64
[37] Cheney M 2001 The linear sampling method and the music algorithm *Inverse Problems* **17** 591–5
[38] Cheney M and Isaacson D 1992 Distinguishability in impedance imaging *IEEE Trans. Biomed. Eng.* **39** 852–60
[39] Cheney M, Isaacson D and Newell J C 1999 Electrical impedance tomography *SIAM Rev.* **41** 85–101
[40] Cherkaev A V and Gibiansky L V 1994 Variational principles for complex conductivity, viscoelasticity, and similar problems in media with complex moduli *J. Math. Phys.* **35** 127–45
[41] Cherkaeva E 2001 Inverse homogenization for evaluation of effective properties of a mixture *Inverse Problems* **17** 1203–18
[42] Cherkaeva E and Tripp A 1996 Inverse conductivity problem for noisy measurements *Inverse Problems* **12** 869–83
[43] Chu M T and Golub G H 2001 Structured inverse eigenvalue problems *Acta Numer.* 1–70
[44] Courant R and Hilbert D 1953 *Methods of Mathematical Physics* vol 1 (New York: Wiley)
[45] Curtis E B, Ingerman D and Morrow J A 1998 Circular planar graphs and resistor networks *Linear Algebra Appl.* **283** 115–50
[46] Curtis E B and Morrow J A 1990 Determining the resistors in a network *SIAM J. Appl. Math.* **50** 931–41
[47] Colin de Verdière Y 1994 Réseaux électriques planaires i *Comments Math. Helv.* **69** 351–74
[48] Colin de Verdière Y 1996 Réseaux électriques planaires ii *Comments Math. Helv.* **71** 144–67
[49] Dennis J E and Schnabel R B 1996 *Numerical Methods for Unconstrained Optimization and Nonlinear Equations* (Philadelphia, PA: SIAM)
[50] Hanoch L-A and Devaney A J 2000 The time reversal technique re-interpreted: subspace based signal processing for multi-static target location *IEEE Sensor Array and Multichannel Signal Processing Workshop (Cambridge, MA)* pp 509–13

[51] Dines K A and Lytle R J 1981 Analysis of electrical conductivity imaging *Geophysics* **46** 1025–36
[52] Dobson D C 1990 Stability and regularity of an inverse elliptic boundary value problem *Technical Report* TR90-14 Rice University, Dept of Math. Sciences
[53] Dobson D C 1992 Convergence of a reconstruction method for the inverse conductivity problem *SIAM J. Appl. Math.* **52** 442–58
[54] Dobson D C 1992 Estimates on resolution and stabilization for the linearized inverse conductivity problem *Inverse Problems* **8** 71–81
[55] Dorn O, Bertete-Aguirre H, Berryman J G and Papanicolaou G C 1999 A nonlinear inversion method for 3d electromagnetic imaging using adjoint fields *Inverse Problems* **15** 1523–58
[56] Dorn O, Bertete-Aguirre H, Berryman J G and Papanicolaou G C 2002 Sensitivity analysis of a nonlinear inversion method for 3d electromagnetic imaging in anisotropic media *Inverse Problems* **18** 285–317
[57] Dorn O, Miller E L and Rappaport C M 2000 A shape reconstruction method for electromagnetic tomography using adjoint fields and level sets *Inverse Problems* **16** 1118–56
[58] Druskin V 1982 The unique solution of the inverse problem of electrical surveying and electrical well-logging for piecewise-continuous conductivity *Izv. Earth Phys.* **18** 51–3
[59] Druskin V 1985 On uniqueness of the determination of the three-dimensional underground structures from surface measurements with variously positioned steady-state or monochromatic field sources *Sov. Phys.–Solid Earth* **21** 210–4 (English transl. (Washington, DC: American Geophysical Union))
[60] Druskin V and Knizherman L 2000 Gaussian spectral rules for second order finite-difference schemes. mathematical journey through analysis, matrix theory and scientific computation *Numer. Algorithms* **25** 139–59
[61] Druskin V and Knizhnerman L 2000 Gaussian spectral rules for three-point second differences: I. A two-point positive definite problem in a semiinfinite domain *SIAM J. Numer. Anal.* **37** 403–22
[62] Druskin V and Moskow S 2002 Three-point finite difference schemes. Padé and the spectral Galerkin method. I. One-sided impedance approximation *J. Math. Comput.* **239** 995–1019
[63] Eggleston M R, Schwabe R J, Isaacson D and Coffin L F 1989 The application of electric current computed tomography to defect imaging in metals *Review of Progress in Quantitative NDE* ed D O Thompson and D E Chimenti (New York: Plenum)
[64] Ekeland I and Témam R 1999 *Convex Analysis and Variational Problems* (Philadelphia, PA: SIAM)
[65] Engl H W, Hanke M and Neubauer A 1996 *Regularization of Inverse Problems* (Dordrecht: Kluwer)
[66] Engl H W, Kunisch K and Neubauer A 1989 Convergence rates for Tikhonov regularization of nonlinear ill-posed problems *Inverse Problems* **5** 523–40
[67] Fannjiang A and Papanicolaou G C 1994 Convection enhanced diffusion for periodic flows *SIAM J. Appl. Math.* **54** 333–408
[68] Folland G B 1995 *Introduction to Partial Differential Equations* (Princeton, NJ: Princeton University Press)
[69] Francini E 2000 Recovering a complex coefficient in a planar domain from the Dirichlet-to-Neumann map *Inverse Problems* **16** 107–19
[70] Colli Franzone P, Guerri L, Taccardi B and Viganotti C 1979 The direct and inverse potential problems in electrocardiology. Numerical aspects of some regularization methods and application to data collected in isolated dog heart experiments *Pub. 222* Laboratorio di Analisi Numerica del Consiglio Nazionale delle Richerche, Pavia
[71] Friedman A and Vogelius M 1989 Determining cracks by boundary measurements *Indiana Univ. Math. J.* **3** 527–56
[72] Gisser D G, Isaacson D and Newell J C 1990 Electric current computed tomography and eigenvalues *SIAM J. Appl. Math.* **50** 1623–4
[73] Golden K and Papanicolaou G 1983 Bounds on effective parameters of heterogeneous media by analytic continuation *Commun. Math. Phys.* **90** 473–91
[74] Gray G 2002 A variationally constrained numerical solution of the electrical impedance tomography problem *Computational and Applied Mathematics PhD Thesis, Technical Report* 02-02 Rice University
[75] Grimmet G 1980 *Percolation* (New York: Springer)
[76] Grünbaum A and Zubelli J P 1992 Diffuse tomography: computational aspects of the isotropic case *Inverse Problems* **8** 421–33
[77] Haber E and Ascher U 2000 Fast finite volume simulation of 3d electromagnetic problems with highly discontinuous coefficients *SIAM J. Sci. Comput.* **22** 1943–61
[78] Haber E and Ascher U 2001 Preconditioned all-at-once methods for large, sparse parameter estimation problems *Inverse Problems* **17** 1847–64
[79] Haber E, Ascher U and Oldenburg D 2000 On optimization techniques for solving nonlinear inverse problems *Inverse Problems* **16** 1263–80

[80] Hadamard J 1902 Sur les problèmes aux dérivées partielles et leur signification physique *Bull. Univ. Princeton* **13**
[81] Halperin B I 1989 Remarks on percolations and transport in networks with a wide range of bond strengths *Physica* D **38** 179–83
[82] Hanke M 1997 Regularizing properties of a truncated Newton–CG algorithm for nonlinear inverse problems *Numer. Funct. Anal. Optim.* **18** 971–93
[83] Harris N D, Suggett A J, Barber D and Brown B 1987 Applications of applied potential tomography (APT) in respiratory medicine *Clin. Phys. Physiol. Meas.* **8** 155–65
[84] Holder D 1993 *Clinical and Physiological Applications of Electrical Impedance Tomography* (London: UCL Press)
[85] Ikehata M and Siltanen S 2000 Numerical method for finding the convex hull of an inclusion in conductivity from boundary measurements *Inverse Problems* **16** 1043–52
[86] Ingerman D 2000 Discrete and continuous Dirichlet-to-Neumann maps in the layered case *SIAM J. Math. Anal.* **31** 1214–34
[87] Ingerman D, Druskin V and Knizhnerman L 2000 Optimal finite-difference grids and rational approximations of the square root. I. Elliptic problems *Commun. Pure Appl. Math.* **53** 1039–66
[88] Isaacson D 1986 Distinguishability of conductivities by electric current computed tomography *IEEE Trans. Med. Imag.* **5** 91–5
[89] Isaacson D and Cheney M 1990 Current problems in impedance imaging *Inverse Problems in Partial Differential Equations* ed D Colton, R Ewing and W Rundell (Philadelphia, PA: SIAM) pp 141–9
[90] Isaacson D and Cheney M 1991 Effects of measurement precision and finite number of electrodes on linear impedance imaging algorithms *SIAM J. Appl. Math.* 1705–31
[91] Isaacson D and Isaacson E 1989 Comment on Calderón's paper: on an inverse boundary value problem *Math. Comput.* **52** 553–9
[92] Isakov V 1993 Uniqueness and stability in multi-dimensional inverse problems *Inverse Problems* **9** 579–621
[93] Isakov V 1998 *Inverse Problems for Partial Differential Equations* (New York: Springer)
[94] Ito K, Kunisch K and Li Z 2001 Level-set function approach to an inverse interface problem *Inverse Problems* **17** 1225–42
[95] Kac I S and Krein M G 1974 On the spectral functions of the string *Am. Math. Soc. Transl. Ser 2* **103** 19–102
[96] Kaipio J P, Kolehmainen V, Somersalo E and Vauhkonen M 2000 Statistical inversion and Monte Carlo sampling methods in electrical impedance tomography *Inverse Problems* **16** 1487–522
[97] Kaipio J P, Kolehmainen V, Vauhkonen M and Somersalo E 1999 Inverse problems with structural prior information *Inverse Problems* **15** 713–29
[98] Kaltenbacher B 2001 On the regularizing properties of a full multigrid method for ill-posed problems *Inverse Problems* **17** 767–88
[99] Keller G V 1988 *Electrical Properties of Rocks and Minerals, Handbook of Physical Constants* ed S P Clarck Jr (New York: Geological Society of America) pp 553–77
[100] Keller J B 1963 Conductivity of a medium containing a dense array of perfectly conducting spheres or cylinders or nonconducting cylinders *J. Math. Phys.* **34** 991–3
[101] Keller J B 1987 Effective conductivity of periodic composites composed of two very unequal conductors *J. Math. Phys.* **28** 2516–20
[102] King J T 1992 Multilevel algorithms for ill-posed problems *Numer. Math.* **61** 313–34
[103] Kirsch A 1998 Characterization of the shape of the scattering obstacle using the spectral data of the far field operator *Inverse Problems* **14** 1489–512
[104] Kohn R V and McKenney A 1990 Numerical implementation of a variational method for electrical impedance tomography *Inverse Problems* **6** 389–414
[105] Kohn R V and Vogelius M 1984 Determining conductivity by boundary measurements *Commun. Pure Appl. Math.* **37** 113–23
[106] Kohn R V and Vogelius M 1984 Identification of an unknown conductivity by means of measurements at the boundary *Inverse Problems (SIAM-AMS Proc. No. 14)* ed D McLaughlin (Providence, RI: American Mathematical Society) pp 113–23
[107] Kohn R V and Vogelius M 1985 Determining conductivity by boundary measurements ii. interior results *Commun. Pure Appl. Math.* **38** 643–67
[108] Kohn R V and Vogelius M 1987 Relaxation of a variational method for impedance computed tomography *Commun. Pure Appl. Math.* **XL** 745–77
[109] Koplik J 1982 Creeping flow in two-dimensional networks *J. Fluid. Mech.* **119** 219–47
[110] Kozlov S M 1989 Geometric aspects of averaging *Russ. Math. Surv.* **44** 91–144

[111] Lee J and Uhlmann G 1989 Determining anisotropic real-analytic conductivities by boundary measurements *Commun. Pure Appl. Math.* **42** 1087–112
[112] Li Yan Yan and Vogelius M 2000 Gradient estimates for solutions to divergence form elliptic equations with discontinuous coefficients *Arch. Rational Mech. Anal.* **153** 91–151
[113] McCormick S F and Wade J G 1993 Multigrid solution of a linearized, regularized least-squares problem in electrical impedance tomography *Inverse Problems* **9** 697–713
[114] Milton G W 1980 Bounds on the complex dielectric constant of a composite material *Appl. Phys. Lett.* **37** 300–2
[115] Morozov V A 1984 *Methods for Solving Incorrectly Posed Problems* (New York: Springer)
[116] Nachman A, Sylvester J and Uhlmann G 1988 An n-dimensional Borg–Levinson theorem *Commun. Math. Phys.* **115** 595–605
[117] Nachman A I 1988 Reconstructions from boundary measurements *Ann. Math.* **128** 531–76
[118] Nachman A I 1996 Global uniqueness for a two-dimensional inverse boundary problem *Ann. Math.* **143** 71–96
[119] Nocedal J and Wright S J 1999 *Numerical Optimization (Springer Series in Operations Research)* (New York: Springer)
[120] Osher S J and Santosa F 2001 Level set methods for optimization problems involving geometry and constraints. i. frequencies of a two-density inhomogeneous drum *J. Comput. Phys.* **171** 272–88
[121] O'Sullivan F 1986 A statistical perspective on ill-posed inverse problems *Stat. Sci.* **1** 502–27
[122] Päivärinta L, Panchencko A and Uhlmann G 2002 Complex geometrical optics solutions for Lipschitz conductivities *Rev. Mat. Iberoamericana* at press
[123] Parker R L 1984 The inverse problem of resistivity sounding *Geophysics* **142** 2143–58
[124] Ramirez A, Daily W, Binley B, LaBreque D and Roelant D 1996 Detection of leaks in underground storage tanks using electrical resistance methods *J. Environ. Eng. Geophys.* **1** 189–203
[125] Ramirez A, Daily W, LaBreque D, Owen E and Chesnut D 1993 Monitoring an underground steam injection process using electrical resistance tomography *Water Resources Res.* **29** 73–87
[126] Santosa F 1995.1996 A level-set approach for inverse problems involving obstacles *ESAIM Controle Optim. Calc. Var* **1** 17–33
[127] Santosa F, Kaup P and Vogelius M 1996 A method for imaging corrosion damage in thin plates from electrostatic data *Inverse Problems* **12** 279–93
[128] Santosa F and Vogelius M 1990 A backprojection algorithm for electrical impedance imaging *SIAM J. Appl. Math.* **50** 216–43
[129] Santosa F and Vogelius M 1991 A computational algorithm for determining cracks from electrostatic boundary measurements *Int. J. Eng. Sci.* **29** 917–38
[130] Schmidt R O 1986 Multiple emitter location and signal parameter estimation *IEEE Trans. Antennas Prop.* **34** 276–80
[131] Schwan H P and Kay C F 1957 The conductivity of living tissues *Ann. NY Acad. Sci.* **65** 1007–13
[132] Davydycheva S, Druskin V and Habashy T An efficient finite-difference scheme for electromagnetic logging in 3-d anisotropic inhomogeneous media *Geophysics* submitted
[133] Seagar A 1983 Probing with low frequency electric currents *PhD Thesis* University of Canterbury, UK
[134] Siltanen S, Mueller J and Isaacson D 2000 An implementation of the reconstruction algorithm of A Nachman for the 2d inverse conductivity problem *Inverse Problems* **16** 681–99
[135] Somersalo E, Cheney M and Isaacson D 1992 Existence and uniqueness for electrode models for electric current computed tomography *SIAM J. Appl. Math.* **52** 1023–40
[136] Somersalo E, Cheney M, Isaacson D and Isaacson E 1991 Layer stripping: a direct numerical method for impedance imaging *Inverse Problems* **7** 899–926
[137] Somersalo E, Isaacson D and Cheney M 1992 A linearized inverse boundary value problem for Maxwell's equations *J. Comput. Appl. Math.* **42** 123–36
[138] Sun Z 1989 On an inverse boundary value problem in two dimensions *Commun. Partial Diff. Eqns* **14** 1101–13
[139] Sun Z 1990 The inverse conductivity problem in two dimensions *J. Diff. Eqns* **87** 227–55
[140] Sun Z and Uhlmann G 1991 Generic uniqueness for an inverse boundary value problem *Duke Math. J.* **62** 131–55
[141] Sylvester J 1990 An anisotropic inverse boundary value problem *Commun. Pure Appl. Math.* **43** 201–32
[142] Sylvester J 1992 A convergent layer stripping algorithm for radially symmetric impedance tomography problem *Commun. Partial Diff. Eqns* **17** 1955–94
[143] Sylvester J and Uhlmann G 1986 A uniqueness theorem for an inverse boundary value problem in electrical prospection *Commun. Pure Appl. Math.* **39** 92–112
[144] Sylvester J and Uhlmann G 1987 A global uniqueness theorem for an inverse boundary value problem *Ann. Math.* **125** 153–69

[145] Sylvester J and Uhlmann G 1988 Inverse boundary value problems at the boundary—continuous dependence *Commun. Pure Appl. Math.* **XLI** 197–219
[146] Sylvester J and Uhlmann G 1991 Inverse problems in anisotropic media. inverse scattering and applications *Contemp. Math.* **122** 105–17
[147] Tikhonov A N and Arsenin V Y 1977 *Solutions of Ill-Posed Problems* ed F John (Washington, DC: Wiley)
[148] Uhlmann G 1999 Developments in inverse problems since Calderón's foundational paper *Harmonic Analysis and Partial Differential Equations (Chicago Lectures in Math.)*(Chicago, IL: University of Chicago Press) pp 295–345
[149] Uhlmann G 2000 Inverse scattering in anisotropic media *Surveys on Solution Methods for Inverse Problems* ed D Colton, H W Engl, A Louis, J R McLaughlin and W Rundell (New York: Springer) pp 235–52
[150] Vozoff K 1991 The magnetotelluric method *Electromagnetic Methods in Applied Geophysics—Applications* ed M N Nabighian (Tulsa, OK: Society of Exploration Geophysicists) ch 8
[151] Wexler A, Fry B and Neumann M 1985 Impedance-computed tomography algorithm and system *Appl. Opt.* **24** 3985–92
[152] White B S, Kohler W E and Srnka L J 2001 Random scattering in magnetotellurics *Geophysics* **1** 188–204
[153] Yorkey T J, Webster J G and Tompkins W J 1987 Comparing reconstruction algorithms for electrical impedance tomography *IEEE Trans. Biomed. Eng.* **34** 843–52